COMILLAS

UNIVERSIDAD PONTIFICIA

ICAI

GRADO EN INGENIERÍA EN TECNOLOGÍAS INDUSTRIALES

TRABAJO FIN DE GRADO

MODELING AND SIMULATION OF A DOUBLY-FED INDUCTION GENERATOR (DFIG)

Autor: Juan Carlos Císcar Múgica

Instructor: Siddharth Raju

Director: Aurelio García Cerrada

Madrid

Junio 2022

Declaro, bajo mi responsabilidad, que el Proyecto presentado con el título *Modeling and simulation of a doubly-fed induction generator (DFIG)* en la ETS de Ingeniería - ICAI de la Universidad Pontificia Comillas en el curso académico 2021/22 es de mi autoría, original e inédito y no ha sido presentado con anterioridad a otros efectos. El Proyecto no es plagio de otro, ni total ni parcialmente y la información que ha sido tomada de otros documentos está debidamente referenciada.

Fdo.:   Juan Carlos Císcar Múgica   Fecha: 20 / 06 / 2022

Autorizada la entrega del proyecto

EL DIRECTOR DEL PROYECTO

Fdo.:   Aurelio García Cerrada   Fecha: 20 / 06 / 2022

GRADO EN INGENIERÍA EN TECNOLOGÍAS INDUSTRIALES

TRABAJO FIN DE GRADO

MODELING AND SIMULATION OF A DOUBLY-FED INDUCTION GENERATOR (DFIG)

Autor: Juan Carlos Císcar Múgica

Instructor: Siddharth Raju

Director: Aurelio García Cerrada

Madrid

Junio 2022

MODELING AND SIMULATION OF A DOUBLY-FED INDUCTION GENERATOR (DFIG)

Autor: Císcar Múgica, Juan Carlos

Director: García Cerrada, Aurelio

Entidades Colaboradoras: Universidad de Minnesota, Twin Cities y ETS de Ingeniería ICAI (Universidad Pontificia Comillas)

RESUMEN DEL PROYECTO

Los generadores de inducción doblemente alimentados (DFIG) se utilizan ampliamente en el sector de la ingeniería eléctrica. El ejemplo más notable de la aplicación de los DFIG son las turbinas eólicas. Cuando se combinan con un convertidor *back-to-back*, los DFIG permiten que las turbinas eólicas funcionen a diferentes rangos de velocidad. En lugar de tener una velocidad fija de la turbina, como ocurría en las primeras turbinas, los DFIG pueden alcanzar varias velocidades óptimas alimentando el rotor con corrientes de diferentes frecuencias. Esto se consigue con unas pérdidas de potencia y un coste reducidos en comparación con otras alternativas.

En la primera parte de este proyecto se comparan varias alternativas a un motor DFIG. En segundo lugar, hacemos un análisis exhaustivo del marco directo y cuadratura (*dq*), y su aplicación a los DFIG. También describimos el control vectorial de este tipo de motores. En tercer lugar, modelamos e implementamos un DFIG en la plataforma Workbench de Sciamble. Simulamos nuestro modelo y analizamos los resultados bajo diferentes condiciones. El modelo incluye una interfaz de electrónica de potencia adecuada, compuesta por un estimador de posición del rotor y dos controladores proporcionales integrales (PI) para la velocidad y las corrientes del rotor.

Palabras clave: controlador PI; estimador MRAS; generadores CS, DD, DFIG y GFC; marco *dq*.

Metodología

El objetivo del proyecto es conocer en profundidad los generadores de inducción doblemente alimentados (DFIG), con la implementación de un modelo y una serie de ejercicios de simulación. La plataforma en la que se implementan y ejecutan todos los modelos es Workbench de Sciamble (Sciamble Corp., 2021).

Además de los DFIG, también se presentan otras tendencias de aerogeneradores. La principal ventaja de los DFIG es que pueden operar a diferentes velocidades, no necesariamente a sus condiciones nominales, dejando margen a muchos escenarios diferentes. Además, cuando se trabaja con un DFIG, es posible controlar la potencia reactiva que se extrae o inyecta a la red (Okedu y Barghash, 2021).

Otras tendencias tecnológicas son, por ejemplo, los generadores de velocidad constante (CS), modelos de generadores tradicionales, que empiezan a estar obsoletos ya que sólo pueden trabajar en condiciones de funcionamiento fijas. La principal ventaja de un CS es su bajo precio y sus costes de mantenimiento. Otra alternativa son los generadores con engranaje y convertidor completo (GFC), que, al contrario que los DFIG, están compuestos por un generador sin engranaje y el convertidor trabaja a pleno rendimiento. El aspecto positivo es que son insensibles a los fallos de la red. También pueden utilizarse generadores de accionamiento directo (DD). Se basan en máquinas síncronas y, aunque sus dimensiones son poco prácticas, tienen una gran eficacia y fiabilidad. Futuros sistemas de generadores son, por ejemplo, los generadores DD superconductores (Lewis y Muller, 2007; Snitchler et al., 2011) y los motores que implementan convertidores parciales y nominales (Wessels et al., 2011).

En este proyecto también se analiza una visión profunda pero práctica de la teoría del marco directo y cuadratura (*dq*). Basándose en la teoría de los motores de inducción, se describen las diferentes ecuaciones de las variables del motor: corrientes, tensiones, flujo y par. También se deriva la matriz de transformación que cambia una referencia trifásica a *dq*, con una descripción matemática breve y simplificada del control vectorial.

Se discuten los estimadores del sistema adaptativo de referencia del modelo (MRAS), aunque no se implementan en las fases posteriores de este proyecto (Parida y Chatterjee, 2014). Son muy potentes ya que pueden estimar la velocidad mecánica y el flujo del rotor de un sistema, pero su aplicación es de cierta complejidad. En cambio, nuestro modelo implementa un estimador de posición del rotor más sencillo (que solo determina las corrientes del rotor y la velocidad mecánica). La principal diferencia entre estos dos estimadores es que un MRAS incorpora un sensor de velocidad que permite realizar un control vectorial utilizando la velocidad estimada del motor.

Este trabajo también incluye un análisis de los DFIG. Éste se simplifica con algunas suposiciones razonables para que pueda entenderse claramente. Se derivan las ecuaciones generales de

corriente y tensión. Se menciona el funcionamiento de los DFIG en el marco *dq* y también se encuentran todas las ecuaciones necesarias (Mohan y Raju, 2021).

A continuación, realizamos el control vectorial en un DFIG. Es posible alinear el marco *dq* en cualquier combinación, de modo que colocamos el eje *d-* en el vector espacial de enlace de flujo del estator, ya que es el método más práctico. Para realizar el control vectorial, tenemos que crear dos controladores Proporcionales Integrales (PI) diferentes: un bucle interior para las corrientes del rotor (para los ejes *d-* y *q-*), y otro bucle exterior para la velocidad mecánica. La idea es que si controlamos la tensión del rotor, podemos controlar la corriente del rotor. Al controlar esta corriente, también podemos controlar el par, que en otras palabras es la velocidad del rotor. Se presentan las funciones de transferencia. Con la incorporación de estos controladores PI, es posible estimar la posición del rotor a través de la velocidad del flujo del estator. Esta velocidad puede describirse como una función de tensiones, corrientes y enlaces de flujo, que son parámetros conocidos.

Una vez expuesta la teoría, se procede a preparar el modelo. Los cálculos se realizan en papel, utilizando las ecuaciones encontradas anteriormente, y toda la simulación se realiza utilizando el Workbench de Sciamble. Hacemos funcionar un DFIG con parámetros habituales. En primer lugar, realizamos una simulación sencilla dando al motor una tensión sinusoidal en el estator y una tensión nula en el rotor. Se crea el modelo del motor, incorporando todas las ecuaciones del DFIG que se han encontrado antes. Gracias a las matrices de transformación adecuadas, podemos obtener los resultados en forma trifásica. Todas las diferentes variables pueden ser calculadas por separado utilizando el circuito equivalente por fase, dando los resultados en vectores espaciales cuando sea apropiado.

Posteriormente, se incluyen el estimador y los controladores PI. Se seleccionan las velocidades de ancho de banda y los márgenes de fase adecuados, y se encuentran los valores de ganancia PI. Nuestro estimador toma como entradas la tensión del estator -que puede ser controlada por el usuario-, la corriente del estator que es una salida del modelo del motor y la velocidad mecánica, permitiendo estimar la posición del rotor. El modelo del DFIG se puede ver a continuación.
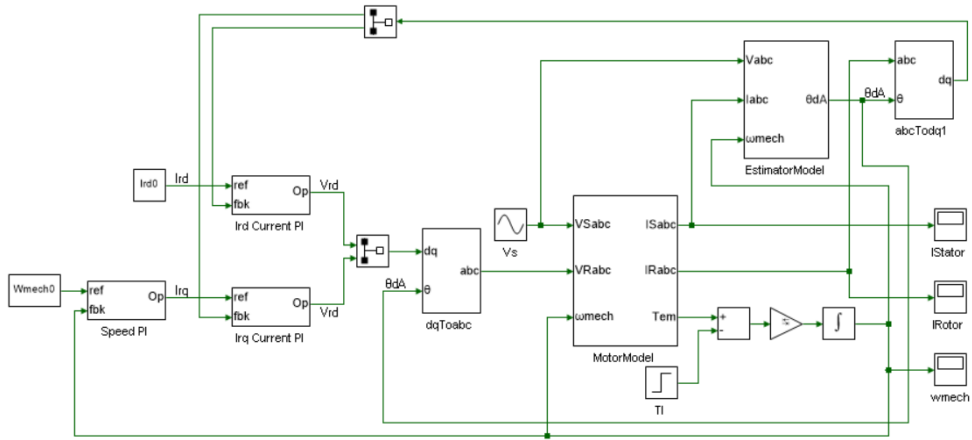
Modelo DFIG. Fuente: elaboración propia en Workbench (Sciamble Corp., 2021)

Resultados

Como simulación final, se estudia la respuesta del sistema cuando se aplica un escalón en el par de carga del 50% del par nominal. Se analizan las corrientes del estator y del rotor, y se comprueba que coinciden con los cálculos realizados anteriormente. También se grafica y examina la velocidad mecánica. El modelo se ejecuta tanto en modo motor como en modo generador (es decir, tomando o suministrando energía a la red). Esto se consigue cambiando el deslizamiento nominal.
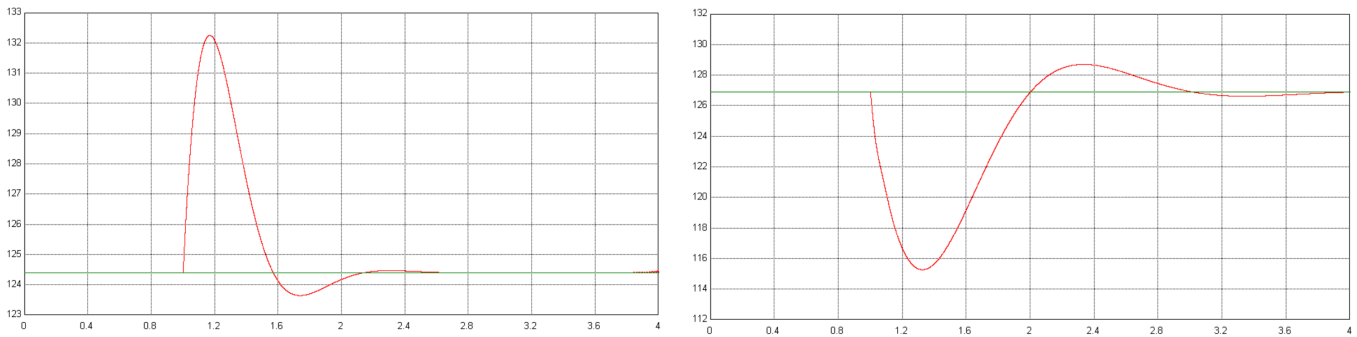
Velocidad mecánica cuando se aplica un escalón de par de carga. Izquierda: modo motor, derecha: generador.

Fuente: elaboración propia en Workbench (Sciamble Corp., 2021)

Se obtienen ondas sinusoidales de amplitud 3185 y 2980 A para las corrientes del estator y del rotor, que giran a 377 y 3.77 rad/s, respectivamente. Se obtiene una velocidad mecánica menor que la velocidad sincrónica en modo motor (124.4 rad/s), y mayor en modo generador (126.9 rad/s).

Conclusiones

La aplicación de los DFIG a las turbinas eólicas está siendo clave para construir un futuro basado en fuentes de energía sostenibles. En este proyecto se analiza, se modela y se simula un DFIG, con una interfaz de electrónica de potencia adecuada. Los valores calculados mediante el circuito equivalente coinciden con los resultados obtenidos en las simulaciones. Se observan las respuestas transitorias de las corrientes del estator y del rotor y la velocidad mecánica.

Sin embargo, este proyecto está limitado ya que consiste en ejercicios de simulación. Comprobar su aplicación en una turbina real tendría un interés muy notable. Las posibles extensiones del proyecto podrían incluir la adición de un filtro de paso bajo a nuestro estimador o el uso de un estimador MRAS. La aplicación de sistemas de generadores modernos, como los DFIG sin escobillas (Brune et al., 1994; Long et al., 2012), también podría analizarse en futuros estudios.

Referencias

Brune C.S., Spee, R. & Wallace, A.K. (1994). Experimental evaluation of a variable speed, doubly-fed wind-power generation system. IEEE Trans. on Industry Applications, pp. 648 – 655.

Lewis, C. & Muller, J. (2007). A direct drive wind turbine HTS generator. IEEE Power Engineering Society General Meeting, pp. 1-8.

Long, T., Shao, S., Abdi, E., Malliband, P., Mathekga, M.E., McMahon, R.A. & Tavner, P.J. (2012). Symmetrical low voltage ride-through of a 250 kW Brushless DFIG. 6th IET Int. Conf. on Power Electronics, Machines and Drives (PEMD).

Mohan N. & Raju S. (2021). Analysis and Control of Electric Drives: Simulations and Laboratory Implementation.

Okedu, K.E. & Barghash, H.F.A. (2021). Enhancing the Performance of DFIG Wind Turbines Considering Excitation Parameters of the Insulated Gate Bipolar Transistors and a New PLL Scheme.

Parida A. & Chatterjee D. (2014). A robust parameter non-sensitive rotor position and speed estimator for DFIG.

Sciamble Corp. (2021). *Workbench*. Desarrollado por Siddharth Raju en la Universidad de Minnesota. Disponible online en: https://sciamble.com/, último acceso: 6 Junio, 2022.

Snitchler, G., Gamble, B., King, C. & Winn, P. (2011). 10 MW class superconductor wind turbine generators. IEEE Trans. on Applied Superconductivity, pp. 1089-1092.

Wessels, C., Gebhart, F. & Fuchs, R.W. (2011). Fault ride-through of a DFIG wind turbine using a dynamic voltage restorer during symmetrical and asymmetrical grid faults. IEEE Trans. on Power Electronics, pp. 807-815.

MODELING AND SIMULATION OF A DOUBLY-FED INDUCTION GENERATOR (DFIG)

Author: Císcar Múgica, Juan Carlos

Director: García Cerrada, Aurelio

Collaborating Entities: University of Minnesota, Twin Cities and ICAI (Universidad Pontificia Comillas)

SUMMARY OF THE PROJECT

Abstract

Doubly-fed induction generators (DFIGs) are widely used all around the electrical engineering sector. The most notable example of the implementation of DFIGs is wind turbines. When combined with a back-to-back converter, DFIGs enable wind turbines to operate at different speed ranges. Instead of having a fixed turbine speed, as early turbines used to, DFIGs can reach various optimal speeds by feeding the rotor with currents of different frequencies. This is done with reduced power losses and cost when compared to other alternatives.

The first part of this project compares various alternatives of DFIGs. Secondly, we do a thorough analysis of the direct and quadrature (*dq*) frame, and its application to DFIGs. We also describe the vector control of this type of motor. Thirdly, we model and implement a DFIG in the Sciamble's Workbench platform. We simulate our model and analyze the results under different conditions. The model includes an appropriate power electronics interface, composed of a rotor position estimator and two Proportional Integral (PI) controllers for the speed and rotor currents.

Key words: CS, DD, DFIG and GFC generators; *dq* frame; PI controller; MRAS estimator.

Methodology

The scope of the project is to deeply understand doubly-fed induction generators (DFIGs), with the implementation of a model and a series of simulation exercises. The platform in which all the models are implemented, and run is Sciamble's Workbench (Sciamble Corp., 2021).

Apart from DFIGs, other wind turbine trends are also presented. DFIG's main advantage is that they can operate at different speeds, not necessarily at their rated conditions, leaving margin to many

different scenarios. In addition, when working with a DFIG, it is possible to control the reactive power that is being drawn or injected to the grid (Okedu and Barghash, 2021).

Other technological trends include for instance constant speed generators (CS), early generator models, which are beginning to be outdated as they can only work at fixed operating conditions. The main advantage of a CS is its low price and maintenance costs. Another alternative is gear and full converter generators (GFC), which, contrary to DFIGs, are composed of a gearless generator and the converter works at full rated conditions. On the positive side, they are insensible to grid faults. Direct-drive generators (DD) can also be used. They are based on synchronous machines and even though their dimensions are a little impractical, they have great efficiency and reliability. Future generator systems are, for example, superconducting DD generators (Lewis and Muller, 2007; Snitchler et al., 2011) and motors that implement partially and fully rated converters (Wessels et al., 2011).

A deep but practical overview of the direct and quadrature (*dq*) frames theory is also discussed in this project. Based on the induction motor theory, the different motor variable equations are described: currents, voltages, flux linkages and torque. The transformation matrix that changes a three-phase to *dq* reference is also derived, with a brief and simplified mathematical description of the vector control.

Even though Model-Reference Adaptative System (MRAS) estimators are not implemented in further phases of this project, they are discussed (Parida and Chatterjee, 2014). They are very powerful as they can estimate the mechanical speed and the rotor flux linkage of a system, but their application is of some complexity. Instead, our model implements a simpler rotor position estimator (which only determines rotor currents and mechanical speed). The main difference between these two estimators is that a MRAS incorporates a speed sensor which makes it possible to perform vector control using the estimated motor speed.

This work also includes an analysis of DFIGs. This is simplified with some reasonable assumptions so that it can be clearly understood. Current and voltage general equations are derived. *Dq* frame operation of DFIGs is mentioned and all the necessary equations can also be found (Mohan and Raju, 2021).

Next, we perform vector control in a DFIG. It is possible to align the *dq* frame in any combination, but we place the *d*-axis in the stator flux linkage space vector, as it is the most practical method. In

order to perform vector control, we have to create two different Proportional Integral (PI) controllers: an inner current loop for the rotor currents (for both *d*- and *q*-axes), and another outer loop for the mechanical speed. The idea is that if we control the rotor voltage, then we can control the rotor current. By controlling this current, we can also control the torque, which in other words is the rotor speed. The transfer functions are presented. With the incorporation of these PI controllers, it is possible to estimate the rotor position through the stator flux linkage speed. This speed can be described as a function of voltages, currents, and flux linkages, which are known parameters.

Once the theory has been exposed, the computer model is set up. The calculations are made on paper, using the equations found before, and all the simulation are done using Sciamble's Workbench. We operate a DFIG with usual parameters. First, we run a simple simulation giving the motor a sinusoidal stator voltage and a zero-rotor voltage. The motor model is created, incorporating all the DFIG equations that have been found before. Thanks to the appropriate transformation matrixes, we can obtain the results in the three-phase form. All the different variables can be calculated separately using the per-phase equivalent circuit, giving the results in space vectors when appropriate.

Later, the estimator and PI controllers are included. Appropriate bandwidth speeds and phase margins are selected, and the PI gain values are found. Our estimator takes the stator voltage -which can be controlled by the user-, the stator current that is an output from the motor model and the mechanical speed as inputs, making it possible to estimate the rotor position. The DFIG model can be seen below.
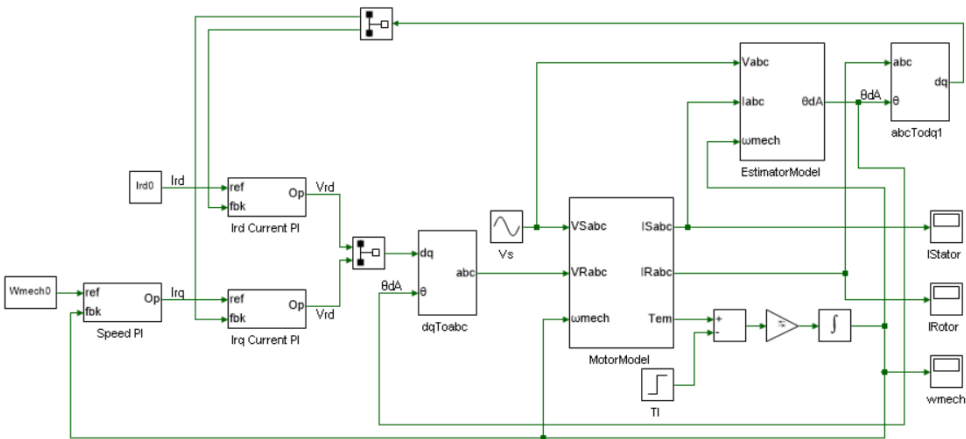
DFIG model. Source: own elaboration in Workbench (Sciamble Corp., 2021)

Results

As a final simulation, we study the response of the system when a step change in the load torque of 50% of the rated torque is applied. The stator and rotor currents are analyzed, and it is verified that they match the calculations that were made before. The mechanical speed is also graphed and examined. The model is run both in motoring and generating mode (i.e., taking or providing power to the grid). This is achieved by changing the rated slip.
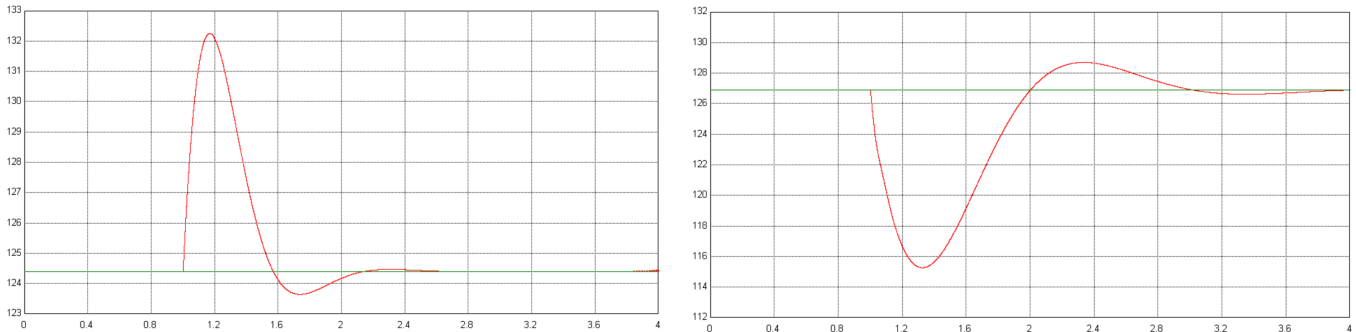
Mechanical speed when a step in load torque is applied. Left: motoring mode, right: generating mode.

Source: own elaboration in Workbench (Sciamble Corp., 2021)

Sinusoidal waves of amplitude 3185 and 2980 A are obtained for stator and rotor currents, rotating at 377 and 3.77 rad/s, respectively. A mechanical speed smaller than the synchronous speed is obtained in motoring mode (124.4 rad/s), and bigger in generating mode (126.9 rad/s).

Conclusions

The application of DFIGs to wind turbines is being key for building a future based on sustainable energy sources. In this project, a DFIG is analyzed, modeled, and simulated, with an appropriate power electronics interface. The calculated values using the per-phase equivalent circuit match the results that are obtained in the simulations. The transient responses of stator and rotor currents and mechanical speed are observed.

However, this project is limited as it consists of simulation exercises. Checking its application in a real-life turbine would be of most notable interest. Possible extensions of the project could include adding a low pass filter to our estimator or using a MRAS estimator instead. The application of modern generator systems, such as brushless DFIGs (Brune et al., 1994; Long et al., 2012), could also be analyzed in future studies.

References

Brune C.S., Spee, R. & Wallace, A.K. (1994). Experimental evaluation of a variable speed, doubly-fed wind-power generation system. IEEE Trans. on Industry Applications, pp. 648 – 655.

Lewis, C. & Muller, J. (2007). A direct drive wind turbine HTS generator. IEEE Power Engineering Society General Meeting, pp. 1-8.

Long, T., Shao, S., Abdi, E., Malliband, P., Mathekga, M.E., McMahon, R.A. & Tavner, P.J. (2012). Symmetrical low voltage ride-through of a 250 kW Brushless DFIG. 6th IET Int. Conf. on Power Electronics, Machines and Drives (PEMD).

Mohan N. & Raju S. (2021). Analysis and Control of Electric Drives: Simulations and Laboratory Implementation.

Okedu, K.E. & Barghash, H.F.A. (2021). Enhancing the Performance of DFIG Wind Turbines Considering Excitation Parameters of the Insulated Gate Bipolar Transistors and a New PLL Scheme.

Parida A. & Chatterjee D. (2014). A robust parameter non-sensitive rotor position and speed estimator for DFIG.

Sciamble Corp. (2021). *Workbench*. Developed by Siddharth Raju at the University of Minnesota. Available online at: https://sciamble.com/, last checked June 6, 2022.

Snitchler, G., Gamble, B., King, C. & Winn, P. (2011). 10 MW class superconductor wind turbine generators. IEEE Trans. on Applied Superconductivity, pp. 1089-1092.

Wessels, C., Gebhart, F. & Fuchs, R.W. (2011). Fault ride-through of a DFIG wind turbine using a dynamic voltage restorer during symmetrical and asymmetrical grid faults. IEEE Trans. on Power Electronics, pp. 807-815.

ACKNOWLEDGEMENTS

Firstly, I would like to thank my tutor Aurelio García for his help throughout the course of this project. His attention and guidance are greatly appreciated.

I would also like to thank the professors I had at the University of Minnesota, Twin Cities, and in particular, Siddharth Raju, whose course EE 5705: Electric Drives in Sustainable Energy Systems I have deeply enjoyed. To Severiano and Sergio for their support during the realization of this project.

Lastly, thanks to my family, for their unconditional support throughout the years.

TABLE OF CONTENTS

FIGURES INDEX

TABLES INDEX

1. INTRODUCTION

In this chapter we set the stage for the work presented in this project. The main interest lies on the implementation in the grid of wind turbines using doubly-fed induction generators (DFIGs). An increase in the development of these technologies can be clearly seen during the last decade. This project will discuss the engineering behind DFIGs.

1.1 Scope and objective

Recently, wind energy has experienced a great advance in its technological development. DFIGs have a major advantage in comparison to other generators as their power converters only need 20-30% of the machine rating for interfacing the rotor and the grid. Moreover, DFIG power converters are cost effective, with low power losses. In addition, they have a good ability to apprehend wind energy, enabling an easy regulation of both active and reactive power (Okedu and Barghash, 2021).

This study aims to further understand DFIG motors, being able to implement one using reasonable parameters. Simulation results are obtained with Sciamble's Workbench, and the adaptation of DFIGs to different external conditions will be studied in order to work with the best performance possible.

1.2 Methodology

Sciamble's platform Workbench (Sciamble Corp., 2021) is the methodology used for the modeling and simulation, a platform ideal for advanced drives simulations as it is possible to create prototypes that can be posteriorly transitioned into large-scale reality.

1.3 Outline of the report

This project contains 5 additional chapters and 4 appendixes:

Chapter 2 provides a brief overview of wind energy, focusing on a brief introduction to DFIGs, and their strengths and weaknesses compared to alternative generator trends, which will also be discussed.

Chapter 3 reviews the *dq* frame. The *dq* frame refers to direct and quadrature axes. In this case, the *d*- and *q*-axes are separated 90° from each other. Only two windings are present, and it simplifies all the calculations of the motor. Different variable equations will be found. MRAS estimator will also be explained, going through how the rotor speed is estimated in detail.

Chapter 4 presents an overview of DFIGs, with a brief analysis of this type of generator and its operation in the *dq* frame. We will also perform vector control of a DFIG, aligning the *d*-axis with the stator flux linkage vector. We will use a rotor position estimator, which will be fully described in this section.

Chapter 5 implements and simulates a DFIG model. The appropriate calculations are done to correctly initialize the motor, which includes a motor, estimator, and PI controller models. The simulation is run and analyzed both in motoring and generating mode.

Chapter 6 summarizes the conclusions and results.

Appendix A describes a short analysis of induction motors (IM). Starting from the structure of an IM, its different variables will be examined. Finally, the per-phase steady-state equivalent circuit will be shown.

Appendix B provides the IM Vector control equations that are continuously being used during the modeling of our motor.

Appendix C includes the simulation script that is used in chapter 5.

Appendix D briefly names and describes the Sustainable Development Goals to which this project is related to.

2. WIND TURBINE TRENDS

DFIGs are one of the most interesting wind turbine technologies but there are other trends. Different alternatives are going to be discussed in this section.

Apart from DFIGs, the most used generator systems applied in wind turbines are constant speed systems with squirrel cage induction generators (CS); brushless generators with gear and full converters (GFC); and direct-drive generator systems (DD). Table 1 lists the top 10 wind turbine manufacturers in 2012 with their characteristics. Fig. 1 shows the different generator systems schemes.

Table 1. Top 10 wind turbine manufacturers in 2012

Manufacturer	Concept	Rotor diameter	Power range
General Electric (US)	DFIG	77 – 120 m	1.5 – 2.85 MW
	DD PM	113 m	4.1 MW
Vestas (Denmark)	DFIG	80 – 100 m	1.8 – 3 MW
	GFC PM	112 – 164 m	1.8 – 8 MW
Siemens (Germany/ Denmark)	GFC IG	82 – 120 m	2.3 – 3.6 MW
	DD PM	101 – 154 m	3 – 6 MW
Enercon (Germany)	DD EE	48 – 126 m	0.8 – 7.5 MW
Suzlon/Repower (India)	CS	52 – 88 m	0.6 – 2.1 MW
	DFIG	95 – 97 m	2.1 MW
Gamesa (Spain)	DFIG	52 – 114 m	0.85 – 2 MW
	GFC PM	128 m	4.5 MW
Goldwind (China)	DD PM	70 – 109 m	1.5 – 2.5 MW
Guodian United	DFIG	77 – 100 m	1.5 – 3 MW
Power (China)	DD PM	100 m	3 MW
Sinovel (China)	DFIG	60 – 113 m	1.5 – 5 MW
MingYang (China)	DFIG	77 – 83 m	1.5 MW
	GFC PM	92 – 108 m	2.5 – 3 MW

Source: Polinder et al., 2013

CS   constant speed with gearbox and induction generator, possibly with two speeds or with extended slip

DFIG   variable speed with gearbox, doubly-fed induction generator and partly rated converter

DD EE   variable speed direct-drive synchronous generator with electrical excitation and full converter

DD PM   variable speed direct-drive permanent-magnet generator and full converter

GFC PM variable speed with gearbox, permanent-magnet generator and full converter

GFC IG   variable speed with gearbox, induction generator and full converter
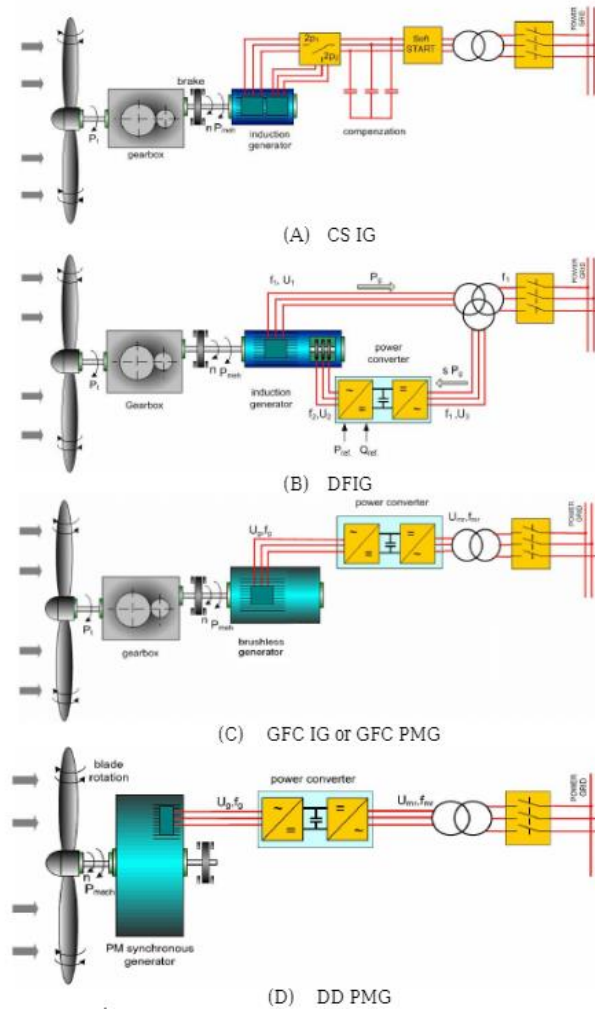
Figure 1. Commonly used generator systems

Source: Ban et al., 2022

2.1 Doubly-fed Induction Generator (DFIG)

In utility-scale wind turbines, common configurations are squirrel-cage induction generators or permanent magnet alternating current (PMAC) generators. These configurations are based on mechanical contacts, such as brushes or slip rings. However, by using DFIGs, there is no need for mechanical contacts and there is total flexibility of the speed of turbine rotation, which is decoupled by a power electronics interface.

In DFIGs, the stator is directly connected to the three-phase grid voltages, while the three-phase windings on the rotor are fed appropriate currents through the power electronics interface. The power electronics interface can also regulate the reactive power that is interacting with the grid. Nevertheless, as the entire power flows through this interface, the control count is very difficult. The power electronics cost is about 7% of the whole wind turbine (Carrasco et al., 2006). Fig. 2 shows the configuration of a DFIG wind turbine generator.
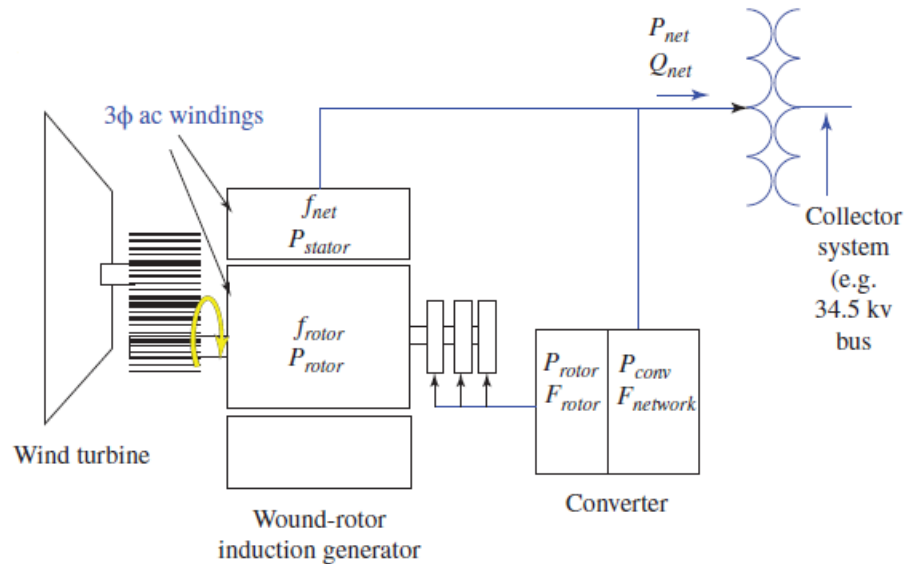
Figure 2. DFIG wind turbine layout

Source: Clark et al., 2010

The benefits of using DFIGs are many. First, it is possible to control the speed over a wide range to make the turbine operate at its optimum coefficient of performance C_p. Secondly, as the stator is connected to the grid, only the rotor is supplied through power electronics. Therefore, the wind turbine does not need to always operate at rated power. Thirdly, they can control the reactive power. However, one of its main disadvantages is that it is very sensible to grid faults. Many

solutions have been proposed, such as the use of distribution static compensator (Phan et al., 2016) or integrating crowbar protection with a battery energy storage system (Endale and Tuka, 2021).

2.2 Constant Speed squirrel cage induction generator (CS)

These systems, also referred to as the Danish concept, has been the most used through the end of the 20th Century. It consists of a three-stage gearbox and a squirrel cage induction connected to the grid. If it is operating above the rated wind speed, the power is limited by the stall effect, such that the power produced by the turbine remains approximately equal to the rated power (Butterfield et al., 1991). Its layout is presented in Fig. 1a.

CS generators are the cheapest and require very low maintenance costs. However, they have poor starting torque and high starting currents. As they cannot be always operating at their optimal conditions, they often present low efficiency.

2.3 Brushless generator with Gear and Full Converter (GFC)

These systems include a gearbox, a brushless generator, and a converter for the full rated power. Different generator types and gearboxes can be used, from permanent magnet to squirrel cage induction generators, as it can be observed in Table 1. Its layout can be seen in Fig. 1c.

Compared to DFIGs, they are not as sensible to grid faults and have less maintenance costs as they have no brushes. On the other hand, converters have more losses because they are fully rated in comparison to DFIGs, which can operate under rated conditions.

2.4 Direct-Drive generator system (DD)

These systems use synchronous machines as generators. In addition, they include a fully rated power electronic converter that will be connected to the grid. Its layout is shown in Fig. 1d.

Their advantages are high efficiency and reliability, with low failure situations and maintenance, as there is no gearbox and have few turbine parts. On the downside, the generators need to be of very big dimensions, with large diameters and mass, and their cost often exceeding.

2.5 Future generator systems

Many investigation studies are being done to improve the previously described systems. Some of the most noticeable ones will be outlined in this subsection.

A gearbox with two output shafts has been proposed, using a mechanical continuously variable transmission (Höhn, 2011; Rossi et al., 2009) and hydrostatic transmissions, being lighter and cheaper than gearboxes (Diepeveen, 2013). A brushless DFIG was suggested by Brune et al., 1994 and a lot of research has been done since (i.e., Long et al., 2012). Different possibilities also exist with improving the power electronic converters, both partially and fully rated (Wessels et al., 2011). Alternative direct-drive generators have also been presented, such as magnetic pseudo (Rens et al., 2010) or superconducting DD generators (Lewis and Muller, 2007; Snitchler et al., 2011).

3. OVERVIEW OF *dq* FRAMES THEORY

3.1 Dynamic analysis in terms of dq-windings

During this subsection, the equations that analyze induction machine operation under dynamic (non-steady state) conditions will be developed. When transforming the three-phase windings into direct and quadrature (*dq*), an intermediary step will be used, in the form of space vectors. The *dq* frame has numerous advantages in controlling AC machines, as it will be seen later in this chapter.

We will be starting from the base that both stator and rotor flux linkages (λ_s and λ_r) depend on the rotor angle (ϑ_m) as the mutual inductances between the stator and rotor windings are dependent on the position. The *dq* analysis allows to control these inductances properly. This can be clearly seen, using for example Park's Transformation. However, a physical approach will be taken in this chapter, enabling the reader to clearly visualize the results.

3.1.1 Stator dq-windings

Take phase currents i_a, i_b, and i_c at a time t, represented by the space vector i_s,

$$i_s(t) = i_a(t) + i_b(t) * e^{j120} + i_c(t) * e^{j240} \tag{3-1}$$

In this situation, the mmf space vector F_s will follow,

$$F_s(t) = \frac{N_s}{p} * i_s(t) \tag{3-2}$$

where N_s equals the number of turns per phase in the three-phase frame and p is the number of poles.

For dynamic analysis and control of AC machines, two orthogonal windings are needed such that the torque and the flux within the machine can be controlled independently. Each orthogonal winding will be sinusoidally distributed with $\sqrt{3/2}\ N_s$ turns. Therefore, we will have one winding along the *d*-axis and the other along the *q*-axis.

The turns factor $\sqrt{3/2}$ could have been any other value. However, it has been chosen so that the *dq*-winding magnetizing inductance is 3/2 of the magnetizing inductance of one phase, as it is proportional to the square of the number of turns,

$$L_{m_{dq}} = \left(\sqrt{\frac{3}{2}}\right)^2 * L_{m_{1ph}} = \frac{3}{2} * L_{m_{1ph}} = L_m \qquad (3\text{-}3)$$

Note that each of these equivalent windings has a resistance R_s and a leakage inductance L_{ls}.

Hence, the magnetomotive force (mmf) produced by the dq-windings will be $\sqrt{3/2}\,\frac{N_s}{p} * (i_{sd} + j *$

$i_{sq})$, where the stator current space vector is expressed using the d-axis as the reference axis. This

way, the stator current can be expressed as $\left(i_{sd} + j * i_{sq}\right) = \sqrt{\frac{2}{3}} * i_s$, which shows that the dq-

winding currents are $\sqrt{2/3}$ times the projection of i_s vector along the d- and q-axes. The factor $\sqrt{2/3}$

ensures that the dq-winding currents produce the same mmf distribution as the three-phase

winding currents.

3.1.2   Rotor dq-windings

The rotor mmf space vector F_r is the produced by the combination of the three-equivalent phase

widings, each with N_s turns.

$$i_r(t) = \frac{F_r(t)}{\frac{N_s}{p}} = i_A(t) + i_B(t) * e^{j120} + i_C(t) * e^{j240} \qquad (3\text{-}4)$$

It should be noted that uppercase nomenclature is being used when referred to the rotor (i.e., *A, B, C*) and lowercase with the stator (i.e., *a, b, c*).

The mmf F_r and the rotor current i_r can also be represented related to the d- and q-axes, as $i_{rd}(t)$ and $i_{rq}(t)$. Both axes are the same that have been chosen for the stator, at it can be observed in Fig.3:
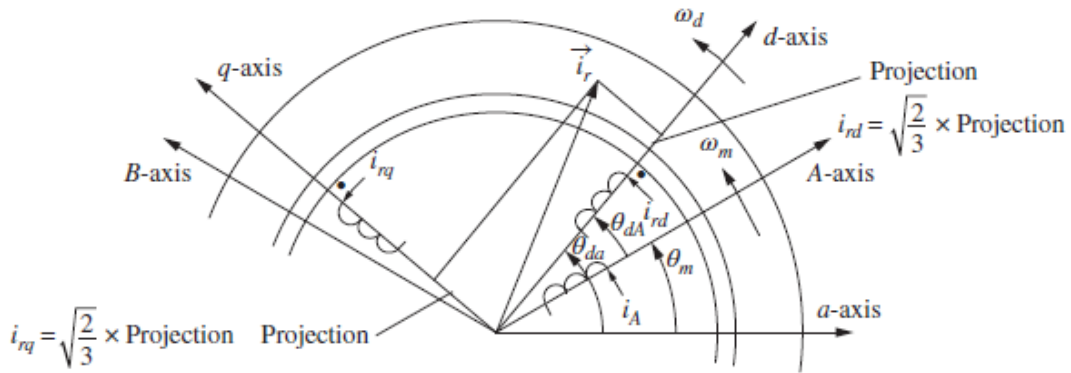
Figure 3. Representation of rotor mmf by equivalent dq-winding currents

32

In this case, the rotor also has $\sqrt{3/2}\ N_s$ turns and a magnetizing inductance of L_m. In addition, each of these rotor equivalent windings has a resistance R_r and a leakage inductance L_{lr}. Fig. 4 shows the stator and rotor representation at any time t.
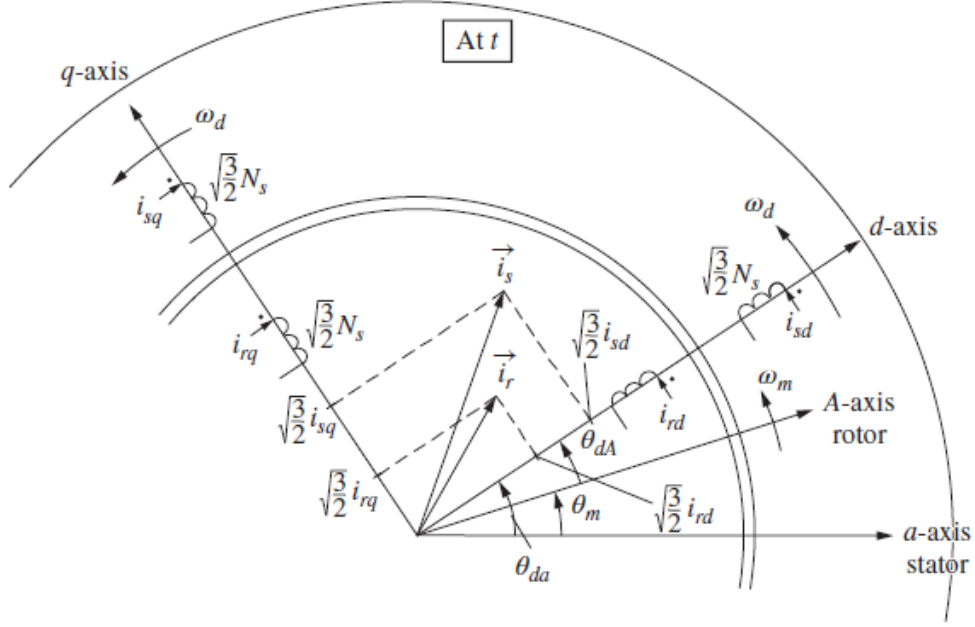
Figure 4. Stator and rotor representation by equivalent dq-winding

The mutual inductances between any *d*-axis and any *q*-axis is zero because of their orthogonal orientation, which results in zero mutual magnetic coupling of flux.

3.1.3   Relation between *dq*-winding and phase winding variables

From Figure 4, we note that at time t, the *d*-axis is at an angle ϑ_{da} with respect to the stator *a*-axis. Therefore, the stator current space vector can be expressed,

$$i_s(t) = i_a(t) * e^{-j\theta_{da}} + i_b(t) * e^{-(j\theta_{da}-120)} + i_c(t) * e^{-(j\theta_{da}-240)} \qquad (3\text{-}5)$$

From the relation $\left(i_{sd} + j * i_{sq}\right) = \sqrt{\dfrac{2}{3}} * i_s$ that was found previously, separating real and imaginary components, the stator current can be described as the following,

33

$$\begin{bmatrix} i_{sd}(t) \\ i_{sq}(t) \end{bmatrix} = \sqrt{\frac{2}{3}} * \begin{bmatrix} \cos(\theta_{da}) & \cos(\theta_{da} - 120) & \cos(\theta_{da} - 240) \\ -\sin(\theta_{da}) & -\sin(\theta_{da} - 120) & -\sin(\theta_{da} - 240) \end{bmatrix} * \begin{bmatrix} i_a(t) \\ i_b(t) \\ i_c(t) \end{bmatrix}$$ (3-6)

where $[T_s]_{abcTOdq}$ will be the transformation matrix to transform stator abc phase winding currents to the corresponding *dq*-winding currents,

$$[T_s]_{abcTOdq} = \sqrt{\frac{2}{3}} * \begin{bmatrix} \cos(\theta_{da}) & \cos(\theta_{da} - 120) & \cos(\theta_{da} - 240) \\ -\sin(\theta_{da}) & -\sin(\theta_{da} - 120) & -\sin(\theta_{da} - 240) \end{bmatrix}$$ (3-7)

Using the same procedure for the rotor currents (now the angle between the *d*-axis with respect to the rotor *A*-axis is θ_{dA},

$$\begin{bmatrix} i_{rd}(t) \\ i_{rq}(t) \end{bmatrix} = \sqrt{\frac{2}{3}} * \begin{bmatrix} \cos(\theta_{dA}) & \cos(\theta_{dA} - 120) & \cos(\theta_{dA} - 240) \\ -\sin(\theta_{dA}) & -\sin(\theta_{dA} - 120) & -\sin(\theta_{dA} - 240) \end{bmatrix} * \begin{bmatrix} i_A(t) \\ i_B(t) \\ i_C(t) \end{bmatrix}$$ (3-8)

where $[T_r]_{abcTOdq}$ will be the transformation matrix to transform for the rotor,

$$[T_r]_{abcTOdq} = \sqrt{\frac{2}{3}} * \begin{bmatrix} \cos(\theta_{dA}) & \cos(\theta_{dA} - 120) & \cos(\theta_{dA} - 240) \\ -\sin(\theta_{dA}) & -\sin(\theta_{dA} - 120) & -\sin(\theta_{dA} - 240) \end{bmatrix}$$ (3-9)

To find the *dq* to three-phase winding matrixes, a row will be added indicating that all three-phase currents add up to zero at any time (assuming an isolated neutral). Inverting the matrix and eliminating the last column as it has no contribution, the following relationships are obtained,

$$\begin{bmatrix} i_a(t) \\ i_b(t) \\ i_c(t) \end{bmatrix} = \sqrt{\frac{2}{3}} * \begin{bmatrix} \cos(\theta_{da}) & -\sin(\theta_{da}) \\ \cos(\theta_{da} + 240) & -\sin(\theta_{da} + 240) \\ \cos(\theta_{da} + 120) & -\sin(\theta_{da} + 120) \end{bmatrix} * \begin{bmatrix} i_{sd}(t) \\ i_{sq}(t) \end{bmatrix}$$ (3-10)

$$\begin{bmatrix} i_A(t) \\ i_B(t) \\ i_C(t) \end{bmatrix} = \sqrt{\frac{2}{3}} * \begin{bmatrix} \cos(\theta_{dA}) & -\sin(\theta_{dA}) \\ \cos(\theta_{dA} + 240) & -\sin(\theta_{dA} + 240) \\ \cos(\theta_{dA} + 120) & -\sin(\theta_{dA} + 120) \end{bmatrix} * \begin{bmatrix} i_{rd}(t) \\ i_{rq}(t) \end{bmatrix}$$ (3-11)

The same way as before, $[T_r]_{dqTOabc}$ is the transform matrix for the stator in the reverse direction and $[T_s]_{dqTOabc}$ for the rotor.

This transformation matrixes also maintain the relation of voltages and flux linkages in the equivalent three-phase and *dq*-windings.

3.1.4   Flux linkage *dq*-windings

The flux linking any winding is due to its own current and that due to the other winding on the same axis,

$$\lambda_{sd} = L_s * i_{sd} + L_m * i_{rd} \tag{3-12}$$

$$\lambda_{sq} = L_s * i_{sq} + L_m * i_{rq} \tag{3-13}$$

$$\lambda_{rd} = L_r * i_{rd} + L_m * i_{sd} \tag{3-14}$$

$$\lambda_{rq} = L_r * i_{rq} + L_m * i_{sq} \tag{3-15}$$

Note that for the simplicity of this document, we will describe the stator inductance as $L_s = L_{ls} + L_m$ and the rotor inductance as $L_r = L_{lr} + L_m$.

3.1.5   *Dq*-winding voltage equations

With the objective of arriving to the voltage equations in the *dq* frame, we will first consider a set of orthogonal αβ windings fixed with the stator (*α*-axis aligned with *a*-axis), as it can be seen in Fig.5.

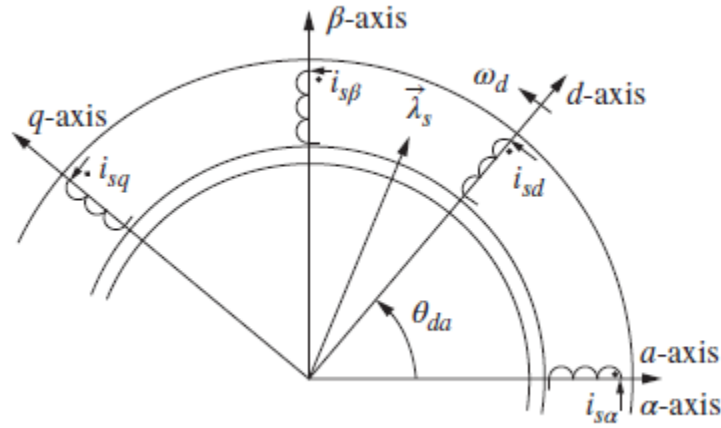*Figure 5. Stator αβ and dq equivalent windings.*

Source: Mohan and Raju, 2021

In terms of the variables of αβ windings, the voltages will be,

$$v_{s\alpha} = R_s * i_{s\alpha} + \frac{d}{dt}\lambda_{s\alpha} \tag{3-16}$$

$$v_{s\beta} = R_s * i_{s\beta} + \frac{d}{dt}\lambda_{s\beta} \tag{3-17}$$

Eqs. 3-16 and 3-17 can be combined resulting in $v_{S_{\alpha\beta}}^{\alpha} = R_s * i_{S_{\alpha\beta}}^{\alpha} + \frac{d}{dt}\lambda_{S_{\alpha\beta}}^{\alpha}$, where $v_{S_{\alpha\beta}}^{\alpha} = V_{s\alpha} + jV_{s\beta}$. The same applies for the rest of the space vectors. Note that the superscript indicates the axis with respect to each variable is being studied.

Using vector projection, $v_{S_{\alpha\beta}}^{\alpha} = v_{S_{dq}}^{d} * e^{j\theta_{da}}$,

$$v_{S_{dq}}^{d} * e^{j\theta_{da}} = R_s * i_{S_{dq}}^{d} * e^{j\theta_{da}} + \frac{d}{dt} * (\lambda_{S_{dq}}^{d} * e^{j\theta_{da}}) \tag{3-18}$$

Expanding and simplifying, we arrive to the following expression,

$$v_{S_{dq}}^{d} = R_s * i_{S_{dq}}^{d} + j * \omega_{da} * \lambda_{S_{dq}}^{d} + \frac{d}{dt} * \lambda_{S_{dq}}^{d} \tag{3-19}$$

where $\omega_{da} = \frac{d}{dt}\theta_{da}$ is the instantaneous speed of the *dq*-windings set in the airgap. Separating the real and imaginary components,

$$v_{sd} = R_s * i_{sd} + \frac{d}{dt}\lambda_{sd} - \omega_{da} * \lambda_{sq} \tag{3-20}$$

$$v_{sq} = R_s * i_{sq} + \frac{d}{dt}\lambda_{sq} + \omega_{da} * \lambda_{sd} \tag{3-21}$$

Repeating the same procedure for the rotor case, but substituting θ_{da} for θ_{dA} as in Fig. 6, we arrive to the following equations,

$$v_{rd} = R_r * i_{rd} + \frac{d}{dt}\lambda_{rd} - \omega_{dA} * \lambda_{rq} \tag{3-22}$$

$$v_{rq} = R_r * i_{rq} + \frac{d}{dt}\lambda_{rq} + \omega_{dA} * \lambda_{rd} \tag{3-23}$$

where $\omega_{dA} = \frac{d}{dt}\theta_{dA}$ is the instantaneous speed of the *dq*-winding set in the air gap with respect to the rotor *A*-axis speed,

$$\omega_{dA} = \omega_{da} - \omega_{m} \tag{3-24}$$

where $\omega_m = \frac{p}{2} * \omega_{mech}$ is the rotor speed in electrical radians per second and ω_{mech} is the rotor speed in actual radians per second.
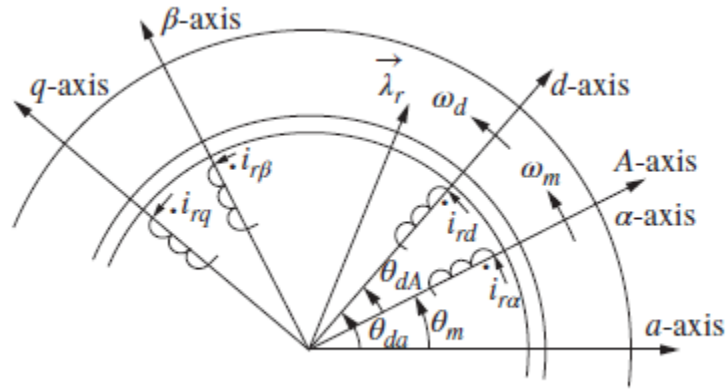
Figure 6. Rotor αβ and dq equivalent windings.

Source: Mohan and Raju, 2021

For future reference through this project, note that $M_{rot} = \begin{bmatrix} 0 & -1 \\ 1 & 0 \end{bmatrix}$ will be used as the rotation matrix for the voltages.

3.1.6   Electromagnetic torque

The peak of the flux density distribution will the mmf multiplied by a constant (which is the airgap permeability divided by its length). The mmf can be found by superposition (Mohan and Raju, 2021), resulting in,

$$B_{rq,pk} = \frac{\mu_0}{l_g} * \frac{\sqrt{\frac{3}{2}} N_s}{p} * \left(i_{sq} + \frac{L_r}{L_m} * i_{rq} \right)$$

(3-25)

Using the torque expression for any sinusoidally distributed windings (Mohan and Raju, 2021),

$$T_{em} = \pi * r * l * \frac{N_s}{2} * B_{r,pk} * i_{s,pk} * \sin(\delta)$$

(3-26)

Noting the current in the rotor *d*-axis winding and the flux due to the *q*-axis, the instantaneous torque on the *d*-axis can be obtained by combining the previous expressions (Eqs. 3-25 and 3-26),

$$T_{em,d} = \frac{p}{2} * \pi * r * l * \frac{\sqrt{\frac{3}{2}}\,N_s}{p} * B_{rq,pk} * i_{rd} = \tag{3-27}$$

$$= \frac{p}{2} * \pi * r * l * \frac{\sqrt{\frac{3}{2}}\,N_s}{p} * \frac{\mu_0}{l_g} * \frac{\sqrt{\frac{3}{2}}\,N_s}{p} * (i_{sq} + \frac{L_r}{L_m} * i_{rq})$$

As we know that $L_m = \frac{3}{2} * \pi * r * \frac{1}{l_g} * \left(\frac{N_s}{p}\right)^2$ and $\lambda_{rq} = L_r * i_{rq} + L_m * i_{sq}$, Eq. 3-27 can be simplified,

$$T_{em,d} = \frac{p}{2} * \lambda_{rq} * i_{rd} \tag{3-28}$$

Similarly, the torque on the *q*-axis will be,

$$T_{em,q} = -\frac{p}{2} * \lambda_{rd} * i_{rq} \tag{3-29}$$

Hence, the net electromagnetic torque on the rotor will be, by superposition,

$$T_{em} = \frac{p}{2} * (\lambda_{rq} * i_{rd} - \lambda_{rd} * i_{rq}) \tag{3-30}$$

3.2 Mathematical description of vector control in induction machines

In vector control, if we align the *d*-axis with respect to the rotor flux linkage, the rotor flux linkage in the *q*-axis will be zero (i.e., $\lambda_{rq} = 0$). With this assumption, it is possible to develop a valid model of the induction machine so that the vector control of induction motor drives can be studied.

However, for the simplicity of this project, these calculations are not going to be shown in this paper. The steps that should be made are substituting the known rotor flux linkage in the *q*-axis in the equations found in the previous section and from there, obtaining the rest of voltages, currents, and rotor fluxes.

The final resulting equations can be found in Eqs. B-11 through B-20 in Appendix B.2.

3.3 Speed-sensorless vector control of induction motor: MRAS estimator

In the previous subsection, the *dq*-frame was chosen to rotate such that the *d*-axis was aligned with respect to the rotor flux linkage. There, the position of the rotor flux linkage space vector is determined from the measured stator currents and the mechanical rotor speed.

There is another way of implementing the motor, which is by adding a speed sensor and therefore performing vector control using estimated motor speed. As the cost of adding a speed sensor is extremely inexpensive, this option is of significant interest. This method only requires the stator current measurement.

The motor speed could also be estimated with an open-loop circuit. However, it presents the shortcoming that it has a high susceptibility to motor parameter variation. Hence, the measured signal presents noise and offset and the estimator is not optimal for many applications in the physical world. A solution for this problem is using a Model-Reference Adaptative System (MRAS) estimator, as it shall be explained below (Parida and Chatterjee, 2014).

3.3.1   Rotor speed estimation

We will use the adaptive speed identification control strategy in order to reduce the effect of the motor parameter variation of the estimated rotor flux linkage space vector position. The rotor flux is estimated independently from the stator and rotor models. The flux linkage, voltage and mechanical equations that are being used can be found in Appendix B.1 in Eqs. B-1 through B-10.

This results in a flexible mechanism that estimates the mechanical speed, so that the result produced by the rotor model follows the one produced by the stator model. The rotor model's output depends on the mechanical speed, hence its adaptivity, whereas the stator model's output is independent from the mechanical speed.

The resulting equations are obtained by combining the IM vector control equations and assuming a static dq-frame ($\omega_{da} = 0$),

$$\frac{d}{dt}\vec{\lambda}^{s}_{r_{dq}} = \frac{L_r}{L_m} * \left(\vec{v}_{s_{dq}} - R_s * \vec{\iota}_{s_{dq}} - \sigma * L_s * \frac{d}{dt}\vec{\iota}_{s_{dq}} \right) \tag{3-31}$$

$$\left(\frac{1}{\tau_r} + \frac{d}{dt} \right)\vec{\lambda}^{r}_{r_{dq}} - j * \omega_m * \vec{\lambda}^{r}_{r_{dq}} = \frac{L_m}{L_r} * R_r * \vec{\iota}_{s_{dq}} \tag{3-32}$$

Where $\sigma = \left(1 - \frac{L_m^2}{L_s * L_r} \right)$ is the leakage factor and $\tau_r = \frac{L_r}{R_r}$ is the rotor time constant, and L_r, L_s and L_m refer to the stator, rotor and magnetizing inductances described in chapter 3.

Note that a superscript s refers to stator model and a superscript r, to rotor model.

The objective of the MRAS is to find the optimal electrical rotor speed ω_m that minimizes the error using both the stator and rotor models, which occurs when function e is minimized (α is the angle between the two estimated rotor flux linkage space vectors),

$$e = \lambda^s_{r_{dq},pk} * \lambda^r_{r_{dq},pk} * \sin \alpha = \lambda^r_{r_d} * \lambda^s_{r_q} - \lambda^r_{r_q} * \lambda^s_{r_d} \tag{3-33}$$

To minimize this error, a PI controller will be designed, in which the output will be ω_m. The method to calculate the controller parameters is described in the following section.

3.3.2   Design of PI controller

The first step will be to obtain the stator d- and q-axis reference currents. Under steady-state conditions and $\lambda_{rq}= 0$ and deriving Eqs. 3-12 and 3-13, reference currents in the stator will be,

$$i_{sd,ref} = \frac{\lambda_{rd,ref}}{L_m} \tag{3-34}$$

$$i_{sq,ref} = \frac{\lambda_{rd,ref}}{L_m} * \omega_{dA} * \tau_r \tag{3-35}$$

The rotor electrical slip speed ω_{dA} needs to be found in order to be able to calculate the stator currents. The rotor electrical slip speed can be obtained from the desired motor speed and the estimated motor speed using a PI controller as the one in Fig. 7 (reference values are represented with a superscript of a star, *). The value of the constant $k = \frac{p}{2} * \frac{L_m^2}{R_r} * i_{sd,ref}^2$, is known from the relationship between ω_{dA} and the electromagnetic torque.

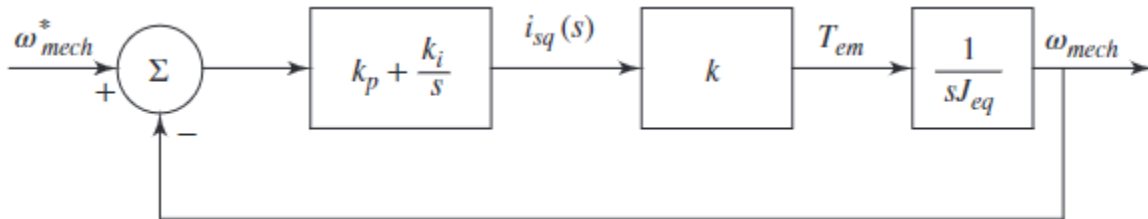*Figure 7. Design of the speed-loop controller*

Source: Mohan and Raju, 2021

This also implies the calculation of θ_{dA}. This way, the rotor flux linkage space vector angle,

$$\theta_{dA} = \int (\omega_m + \omega_{dA}) dt \tag{3-36}$$

The overall system of θ_{dA} and $i_{sq,ref}$ determination based on the estimation of the electrical rotor speed ω_m is shown in Fig. 8. Consequently, the ω_m settles down to the value that makes the rotor flux linkage that has been estimated by the rotor model be the same to the one estimated by the stator model. This is the optimal value as it allows the motor to operate under the maximum torque.
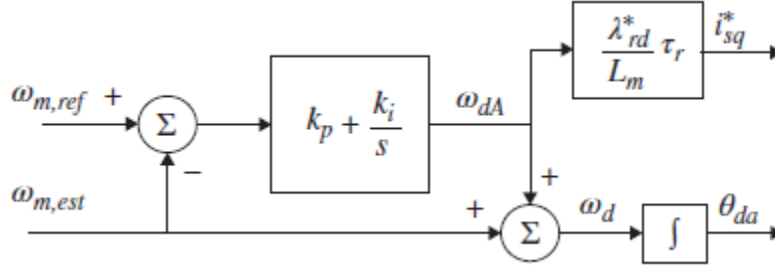

Figure 8. MRAS θ_{dA} and $i_{sq,ref}$ determination

Source: Mohan and Raju, 2021

Going back to the error function e, as it is nonlinear, the controller is tuned of for a linearized model around a steady-state operating point. For a small perturbation in the estimated rotor speed $\Delta\omega_m$, the transfer function will be the following, as it can be observed in Fig. 9,

$$\frac{\Delta e}{\Delta\omega_m} = G(s) = \lambda_{r_{dq},pk,ss}^2 * \frac{\left(s + \dfrac{1}{\tau_r}\right)}{\left(s + \dfrac{1}{\tau_r}\right)^2 + \omega_{slip,ss}^2} \qquad (3\text{-}37)$$
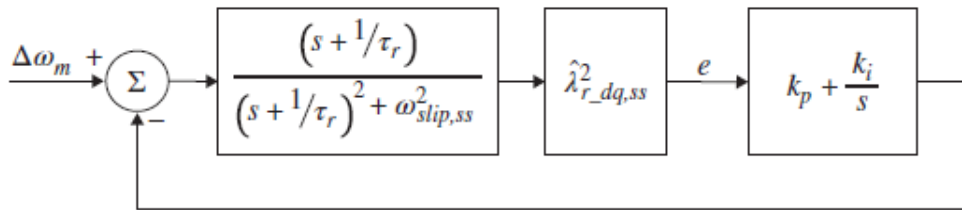
Figure 9. MRAS estimator linearized system transfer function.

Source: Mohan and Raju, 2021

A MRAS estimator will not be implemented in this project. As it has been seen, it is very powerful as it estimates the motor mechanical speed and the rotor flux linkage space vector with high stability across a broad operating condition. Therefore, the implementation of a MRAS estimator is very interesting for possible further extensions of this project. The estimator that will be used in this

project will be explained in detail in the following chapter. Further analysis on MRAS estimators and their limitations can be found in Holtz (2002).

4. OVERVIEW OF DFIGs

DFIGs consist of a stator with a three-phase winding, each with N_s turns per-phase, sinusoidally distributed. Additionally, the rotor consists of a *wye*-connected three-phase winding, each with N_r also sinusoidally turns per-phase. The cross-section of a DFIG can be observed in Fig. 10.
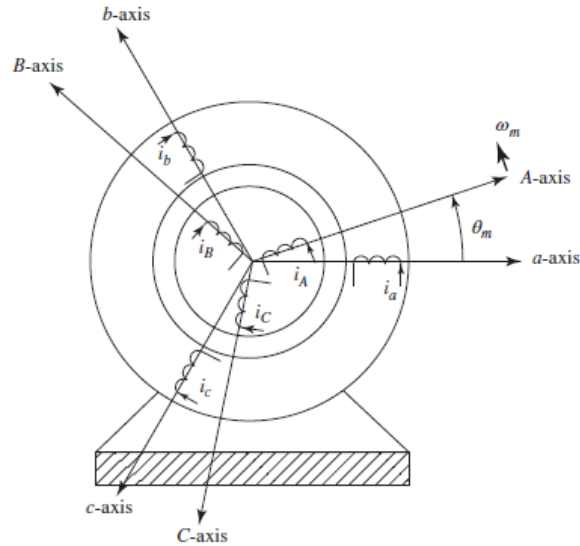
Figure 10. Cross-section of a DFIG

Source: Mohan and Raju, 2021

4.1 Analysis of DFIGs

In this subsection, we are going to realize an analysis of a DFIG in steady state. The assumptions that will be made to simplify the study of DFIGs are the following. First, we will assume that we are operating under a balanced sinusoidal steady-state condition, with the stator connected to 60 Hz grid frequency voltages. Secondly, we will assume a 2-pole machine (note that in the latter chapters we will be using a 6-pole machine) and discard the parasitics (stator resistance R_s and stator leakage inductance L_{ls}).

If phase-*a* voltage peaks at $\omega t = 0$, the space vector diagram is represented in Fig. 11. It follows the induction motor theory that can be found in Appendix A.

Figure 11. DFIG space vector diagram

Source: Mohan and Raju, 2021

The induced back-emf in the stator (e_s) and rotor (e_r) windings can be represented by the following space vectors at $t = 0$ (Mohan and Raju, 2021),
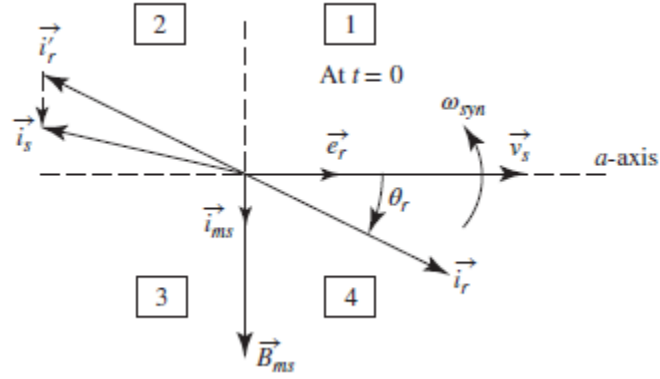
$$e_s = v_s = \left(k_e * B_{ms,pk} * N_s * \omega_{sync}\right) \angle 0° \qquad (4\text{-}1)$$

$$e_r = \left(k_e * B_{ms,pk} * N_r * \omega_{slip}\right) \angle 0° \qquad (4\text{-}2)$$

where:

- k_e represents the electrical constant
- $B_{ms,pk}$ is the peak value of the stator current flux
- ω_{sync} is the synchronous speed with which all the space vector are rotating, with respect to the stationary stator windings
- ω_m is the rotor speed
- $\omega_{slip} = \omega_{sync} - \omega_m$ represents the slip speed

The rotor current space vector can be controller when appropriate slip-frequency voltages (v_r) are applied from the power-electronic converter, as it can be seen in Fig. 12 (at slip frequency),

$$i_r = \frac{v_r - e_r}{R_r + j * \omega_{slip} * L_{lr}} \qquad (4\text{-}3)$$
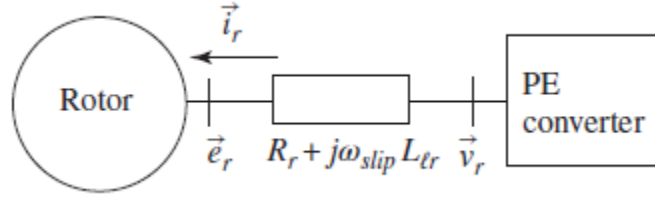
Figure 12. Rotor circuit diagram

Source: Mohan and Raju, 2021

Following the induction motor theory in Appendix A (Eqs. A-10 and A-11), the current drawn from and going into the stator are described by Eqs. 4-2 and 4-3, respectively,

$$i'_r = -\frac{N_r}{N_s} * i_r \tag{4-4}$$

$$i_s = i_{ms} + i'_r \tag{4-5}$$

Based on the vector diagram of Fig. 11, the real and active power into the stator and rotor will be,

$$P_s = \frac{2}{3} * v_{s,pk} * i'_{r,pk} * \frac{N_r}{N_s} * \cos\theta_r \tag{4-6}$$

$$Q_s = \frac{2}{3} * v_{s,pk} * i'_{r,pk} * \frac{N_r}{N_s} * \sin\theta_r \tag{4-7}$$

$$P_r = \frac{2}{3} * s * v_{s,pk} * i'_{r,pk} * \frac{N_r}{N_s} * \cos\theta_r \tag{4-8}$$

$$Q_r = \frac{2}{3} * v_{s,pk} * i'_{r,pk} * \frac{N_r}{N_s} * \sin\theta_r \tag{4-9}$$

where θ_r is the angle between stator voltage and rotor current space vectors. These power flows are represented in Fig. 13.
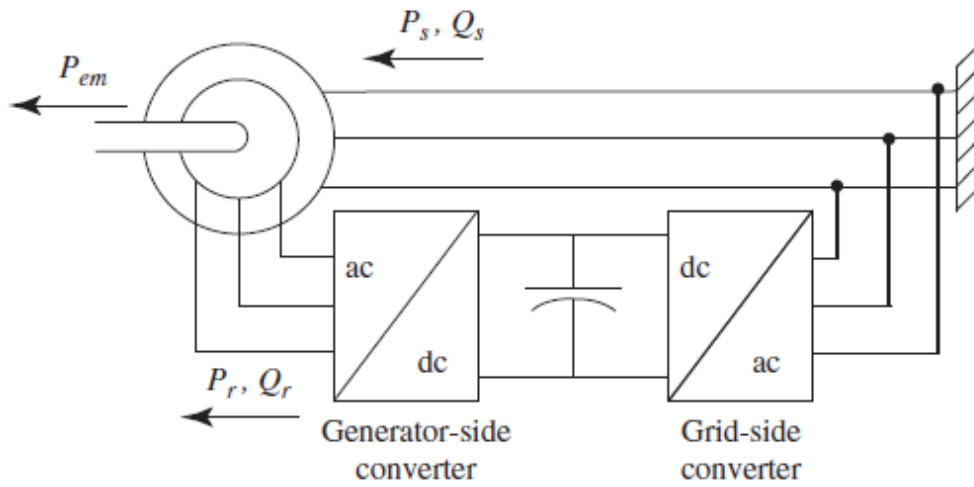
Figure 13. Power flow representation in a DFIG

Source: Mohan and Raju, 2021

4.2 DFIG operation in dq frame

The *dq* analysis is going to be made assuming steady state, neglecting parasitics and with the same number of turns in the rotor and stator ($N_r = N_s$). We will also assume that the *d*-axis is aligned with the rotor flux linkage space vector, such that the rotor flux linkage in the *q*-axis is zero (i.e., $\lambda_{rq} = 0$). A fraction of the cross-section of the motor is shown in Fig. 14.
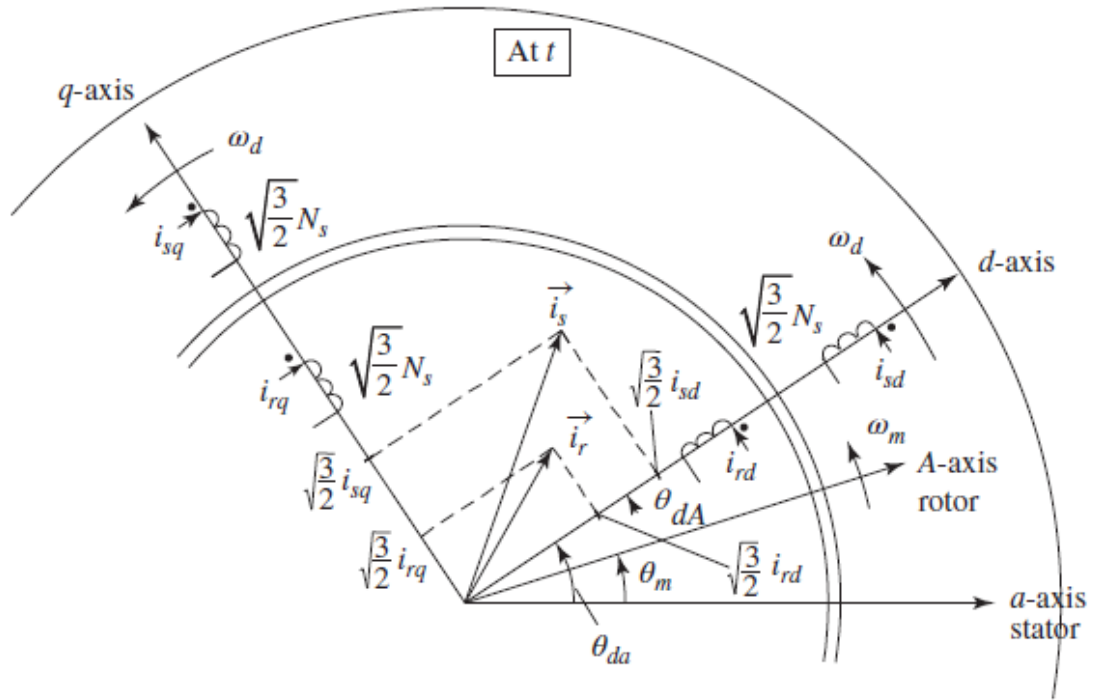
Figure 14. Cross-section of DFIG with d-axis aligned with the rotor flux

Source: Mohan and Raju, 2021

It should be noted that as we have neglected the leakage fluxes., the flux linkages in the stator d-axis will be the same as in that in the rotor d-axis (i.e., $\lambda_{sq} = \lambda_{rq} = 0$). This is for simplification purposes only. When the model is implemented and simulated later in this document, parasitics will be included so this condition will not be satisfied. The IM vector control equations can be found in Appendix B.2.1.

4.3 Vector control of DFIG

In controlling DFIG, it is common to align the d-axis with the stator flux-linkage vector since this leads to significant simplification in the controller design (Brekken, 2005). This methodology will be the same as the one we will realize through the following chapters of this project. The vector control block diagram that is going to be used along this subsection is presented in Fig. 15.

Figure 15. DFIG vector control block diagram

Source: Mohan and Raju, 2021

4.3.1 Rotor current controller

Substituting the flux linkage equations in the rotor voltage equations (Eqs. 3-22 and 3-23),

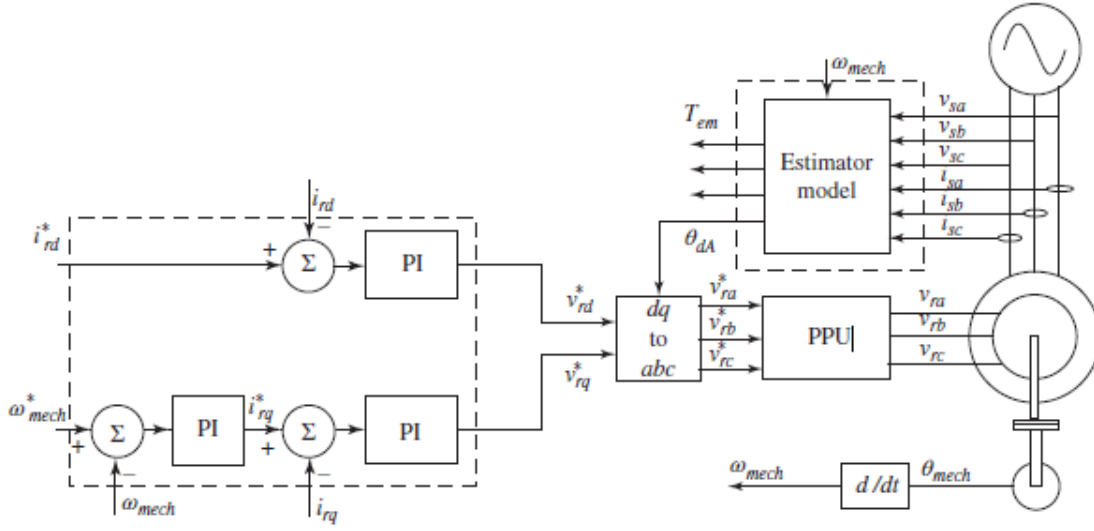$$v_{rd} = R_r i_{rd} + \sigma L_r \frac{di_{rd}}{dt} - \omega_{dA} \sigma L_r i_{rq} + \frac{L_m}{L_s} \frac{d\lambda_{sd}}{dt} \tag{4-10}$$

$$v_{rq} = R_r i_{rq} + \sigma L_r \frac{di_{rq}}{dt} - \omega_{dA} \sigma L_r i_{rd} + \omega_{dA} \frac{L_m}{L_s} \lambda_{sd} \tag{4-11}$$

The voltage drop due to the stator resistance is negligible compared to the applied stator terminal voltage. Therefore, it can be assumed that the stator flux linkage is mainly dominated by the stator voltage. As the grid voltage magnitude is a constant, the stator flux linkage will also be a constant. This way, the last term in Eq. 4-10 can be considered zero and the last term in Eq. 4-11 will be a constant external offset and ignored in the controller design. The cross-coupling terms $\omega_{dA} \sigma L_r i_{rq}$ and $\omega_{dA} \sigma L_r i_{rd}$ can be ignored as disturbances. Therefore, the inner current loop system transfer functions from Eqs. 4-10 and 4-11 are,

$$i_{rd}(s) = \frac{1}{R_r + s\sigma L_r} * v'_{rd}(s) \tag{4-12}$$

$$i_{rq}(s) = \frac{1}{R_r + s\sigma L_r} * v'_{rq}(s) \tag{4-13}$$

4.3.2   Rotor speed controller

The current loop that has been described in the previous subsection needs to be extended with a PI controller to control the rotor speed. This is because in a typical wind-turbine generator, the speed of the turbine is adjusted based on the wind speed to optimize the amount of energy collected from the wind (Tewari et al., 2011).

From the rotor flux equations (Eqs. 3-12 through 3-15), the electromagnetic torque can be expressed as $T_{em} = \frac{p}{2} * \lambda_{sd} * i_{sq}$, since $\lambda_{sq} = 0$, $i_{rq} = -\frac{L_m}{L_s} * i_{sq}$. Combining both expressions, the rotor q-axis current can control the torque, meaning that the rotor speed can also be controlled,

$$T_{em} = -\frac{p}{2} * \frac{L_m}{L_s} * \lambda_{sd} * i_{rq} = k_t * i_{rq} \tag{4-14}$$

where k_t represents the constant value that multiplies the rotor q-axis current to obtain the electromagnetic torque.

4.3.3   Rotor position estimator

From the stator voltage (Eq. 3-20), it is possible to control the stator d-axis flux and the stator flux linkage speed. From the speed, it is possible to compute the rotor flux linkage space vector angle θ_{dA}, as we will later operate in chapter 5.

$$\lambda_{sd} = \int (v_{sd} - R_s * i_{sd})\, dt \tag{4-15}$$

$$\omega_{da} = \frac{v_{sq} - R_s * i_{sq}}{\lambda_{sd}} \tag{4-16}$$

$$\theta_{dA} = \int \omega_{dA}\, dt = \int (\omega_{da} - \omega_{mech})\, dt \tag{4-17}$$

Note that the equation for λ_{sd} involves open integration, which could derive to problems when it comes to practical implementations, as the integrator leads to a gradual accumulation of any offset present in the system and could lead to a non-converging result. This can be fixed replacing the integrator with a low-pass filter. As we do not want to get into a very complicated model, this technique will not be implemented in this project.

5. MOTOR MODELING AND SIMULATION

In this chapter, DFIG is going to be modelled and simulated in Workbench (Sciamble Corp., 2021).

In chapter subsection 5.1 the initial parameters for the motor will be established. In subsection 5.2, the motor will be implemented in the three-phase and *dq* frames. The simulation of the model will be realized in subsection 5.3. In subsection 5.4, we will calculate the initializing values for the integrators used in the model. These values will be checked in subsection 5.5 to ensure that we are following the correct steps. The PI controller will be designed in subsection 5.6. Lastly, the controller will be added to the model, and we will simulate the model in motoring mode in subsection 5.7 and in generating mode in 5.8.

5.1 Initial parameters

To start with, the following initial parameters have been chosen at rated operating conditions. This decision has been made in accordance with usual values of a DFIG (Smajo et al., 2005; and Ozsoy et al., 2014):

$$P = 6 - Number\ of\ poles$$

$$X_{m-1ph} = 573.33\ m\Omega - Per\ phase\ magnetizing\ reactance$$

$$X_{ls} = 50\ m\Omega - Stator\ leakage\ reactance$$

$$X'_{lr} = 47\ m\Omega - Reflected\ rotor\ (as\ seen\ from\ the\ stator)\ leakage\ reactance$$

$$R_s = 2\ m\Omega - Stator\ resistance$$

$$R'_r = 1.5\ m\Omega - Reflected\ rotor\ (as\ seen\ from\ the\ stator)\ resistance$$

$$J = 70\ kg \cdot m^2 - Rotor\ moment\ of\ inertia$$

$$s = 1\% - Slip$$

The motor is connected to a three-phase grid whose characteristics are:

$$f = 60\ Hz - Grid\ frequency$$

$$V = 690\ V - Grid\ line\ line\ RMS\ voltage$$

5.2 Motor modeling in three-phase and *dq* frames

The inputs of the motor model are the stator and rotor voltages and the mechanical speed. The stator voltage will be the grid line-line RMS voltage multiplied by a factor of √2/ √3 separated by 120° for each phase (*a*, *b*, *c*). As in a DFIG there are more variables than control parameters, there are infinite rotor voltages for any given stator voltage, frequency, torque, and speed. For the simplicity of the model, a value of 0 V is being selected for the rotor voltage. On the other hand, the outputs are both stator and rotor currents and the electromagnetic torque. The motor model can be seen in Figs. 16 and 17.

The model includes different subsystems for the stator and rotor flux linkage (Figs. 18 and 19, respectively) and follows DFIG equations (see Eqs. B-1 through B-10 in Appendix B), operating both in three-phase and *dq* frames. This is possible thanks to subsystems that will enable the *abc* into *dq* conversion, and vice versa, as it can be seen in Figures 20 and 21, respectively. This follows Eqs. 3-7 and 3-9, found in chapter 3.
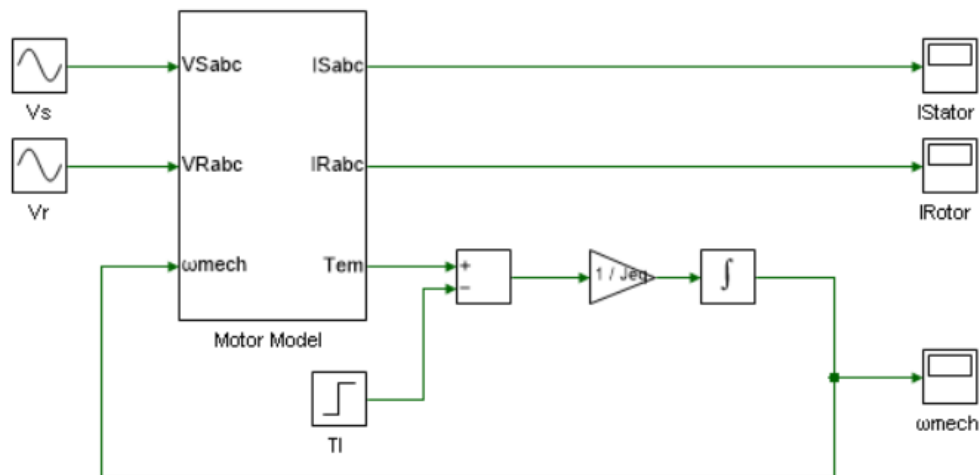
Figure 16. Model in abc and dq reference frames

Source: own elaboration in Workbench (Sciamble Corp., 2021)

Figure 17. Motor model

Source: own elaboration in Workbench (Sciamble Corp., 2021)

Figure 18. Stator flux linkage subsystem

Source: own elaboration in Workbench (Sciamble Corp., 2021)

Figure 19. Rotor flux linkage subsystem
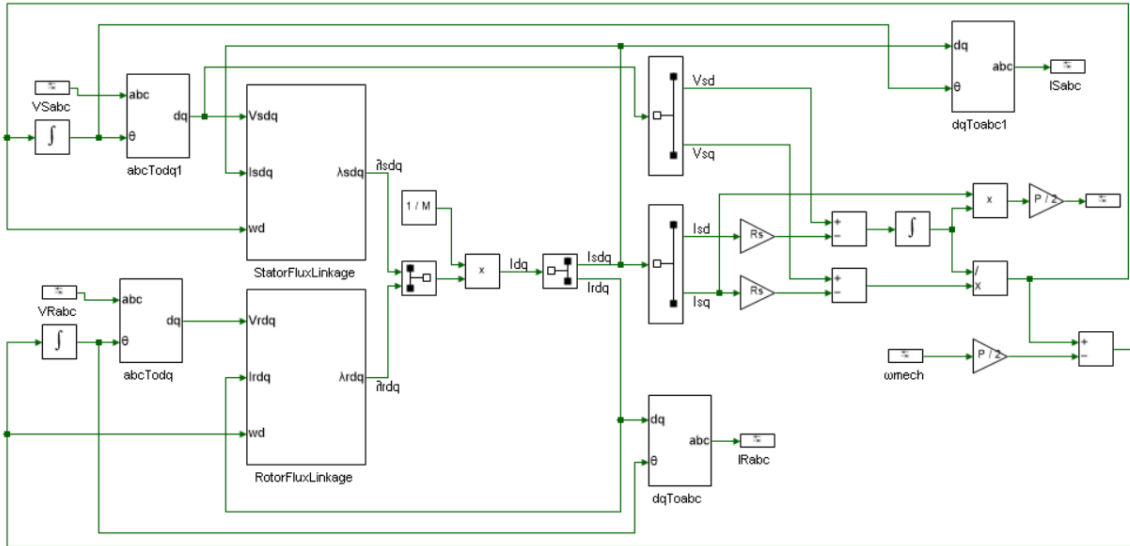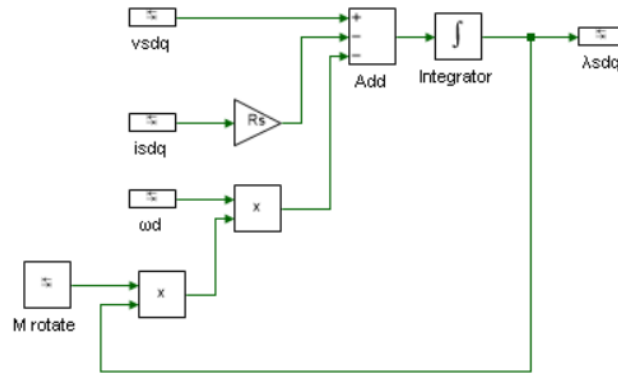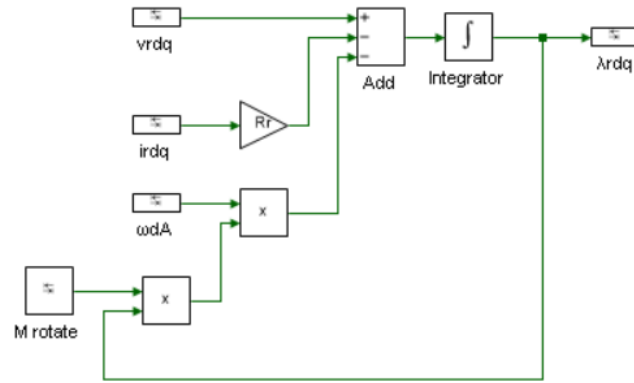
Source: own elaboration in Workbench (Sciamble Corp., 2021)
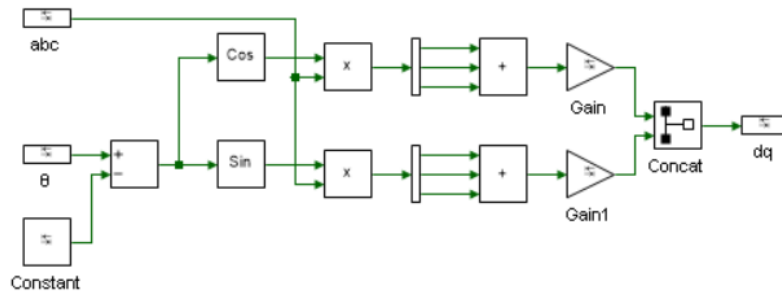
Figure 20. abc to dq frame subsystem conversion

Source: own elaboration in Workbench (Sciamble Corp., 2021)
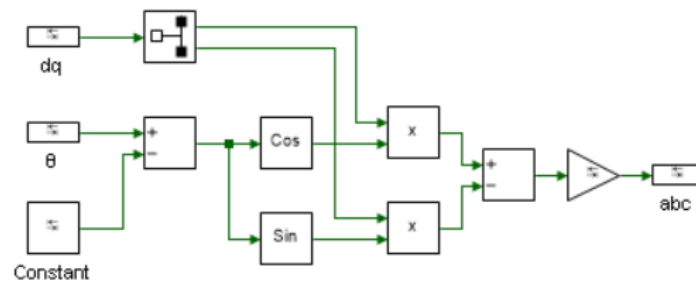
Figure 21. dq to abc frame subsystem conversion

Source: own elaboration in Workbench (Sciamble Corp., 2021)

5.3 Simulation in three-phase and dq frames

5.3.1 Computations

Firstly, variables such as currents, voltages, speed, torque, input and output power and power losses of the motor will be calculated using the induction motor per-phase equivalent circuit model, which can be seen in Fig. 39 in Appendix A. All the formulas that are being used in this subsection can be revisited in the same appendix.

a. Stator current

$$I_{s,pk} = 3185.47\angle - 41.1° \text{ A}$$

$$I_a = 3185.47 * \sin(\omega_e t - 41.1°)\, A$$

$$I_b = 3185.47 * \sin(\omega_e t - 41.1° - 120°)\, A$$

$$I_c = 3185.47 * \sin(\omega_e t - 41.1° - 240°)\, A$$

where $\omega_e = 376.99\ rad/s$ is the electrical frequency, with which stator currents rotate.

b. Voltages across magnetizing inductance

$$V_{m,pk} = 468.42\angle - 14.32° \text{ V}$$

$$V_{m,a} = 468.42 * \sin(\omega_e t - 14.32°)\, V$$

$$V_{m,b} = 468.42 * \sin(\omega_e t - 14.32° - 120°)\, V$$

$$V_{m,c} = 468.42 * \sin(\omega_e t - 14.32° - 240°)\, V$$

where $\omega_e = 376.99\ rad/s$ is the electrical frequency, with which these voltages rotate.

c. Ratio of Magnetizing current to total stator current

$$I_{m,pk} = 544.67\angle - 104.32° \text{ A}$$

$$\%magnetizing\ current = \frac{|I_m|}{|I_s|} * 100 = 17.1\%$$

d. Induced rotor voltages

$$E_{r,pk} = 4.68\angle - 14.32° \text{ V}$$

$$E_{r,a} = 4.68 * \sin(\omega_r t - 14.32°) \, V$$

$$E_{r,b} = 4.68 * \sin(\omega_r t - 14.32° - 120°) \, V$$

$$E_{r,c} = 4.68 * \sin(\omega_r t - 14.32° - 240°) \, V$$

where $\omega_r = s * \omega_e = 3.77 \, rad/s$ is the rotor voltage frequency, with which rotor voltages rotate.

e. Rotor currents

$$I_{r,pk} = 2979.92\angle - 31.71° \text{ A}$$

$$I_{r,a} = 2979.92 * \sin(\omega_r t - 31.71°) \, A$$

$$I_{r,b} = 2979.92 * \sin(\omega_r t - 31.71° - 120°) \, A$$

$$I_{r,c} = 2979.92 * \sin(\omega_r t - 31.71° - 240°) \, A$$

$$\omega_r = 3.77 \, rad/s$$

where $\omega_r = s * \omega_e = 3.77 \, rad/s$ is the rotor frequency, with which rotor currents rotate.

f. Motor speed

$$\omega_m = 124.41 \, rad/s$$

g. Output power

$$P_o = 1978 \, kW$$

h. Input real and reactive power

$$P_{in} = 2028 \, kW$$

$$Q_{in} = 1770 \; kvar$$

i. Electromagnetic torque

$$T_{em} = 15889.46 \; Nm$$

j. Power losses
   1. Stator resistance

$$P_{loss,stator} = 30.44 \; kW$$

   2. Rotor resistance

$$P_{loss,rotor} = 19.98 \; kW$$

   3. Total loss

$$P_{loss,total} = 40.42 \; kW$$

k. Efficiency

$$\eta = \frac{P_{out}}{P_{in}} * 100 = 97.5\%$$

5.3.2 Simulation

The simulations will be made using the Euler solver, as it has enough power, and a more complex solver would only slow down the simulations. The circuit is being studied when the model is being operated under rated grid voltage starting from time t = 0, and a step change in load torque to 25% of its rated torque at time t = 15 seconds. The simulation time has been selected to be 20 seconds. This decision will be explained once the results are presented. The step time selected has been 5 μs. Although it is a very small value, a bigger value does not measure the torque and speed correctly.

The simulation results for the stator and rotor currents are shown in Fig. 22 and 23 (note that color red represents *a*-phase; green *b*-phase; and blue *c*-phase). Fig. 24 represents the electromagnetic and load torques (color green represents electromagnetic torque; and red, load torque) and Fig. 25, the mechanical speed.

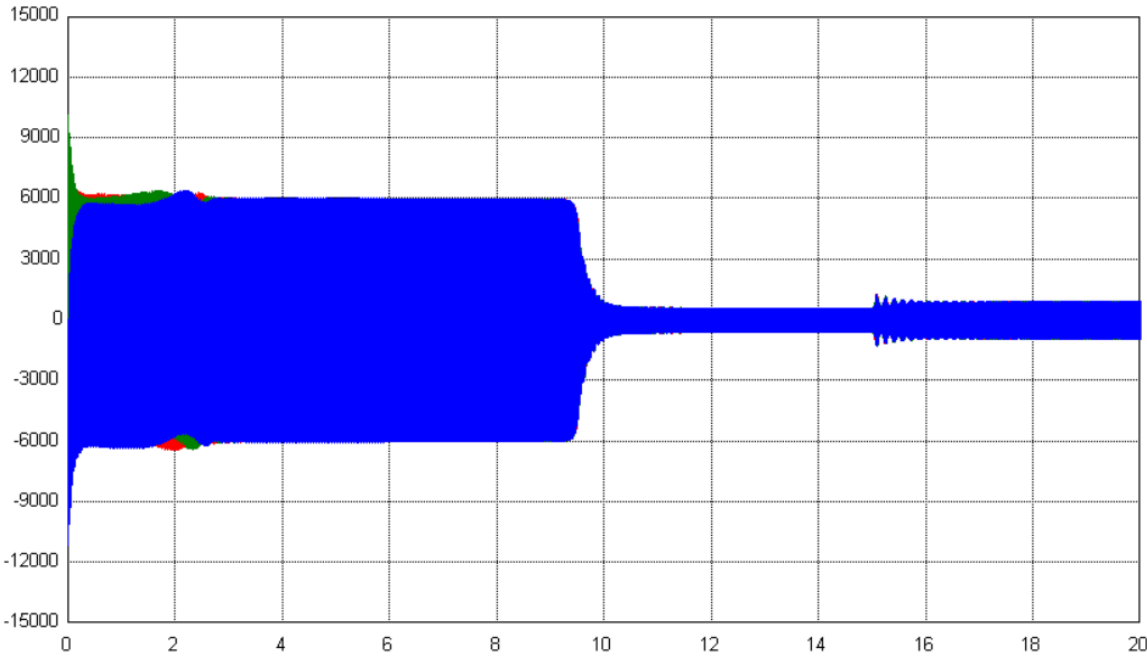*Figure 22. Stator currents (step in load torque of 25% rated torque)*

Source: own elaboration in Workbench (Sciamble Corp., 2021)
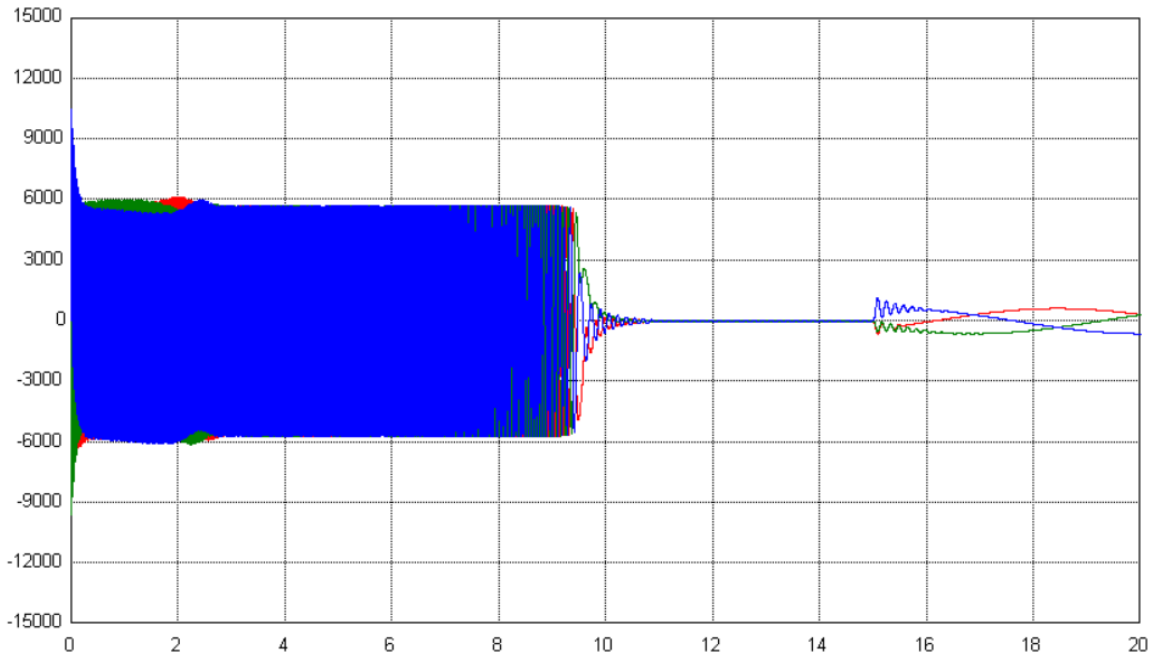
Figure 23. Rotor currents (step in load torque of 25% rated torque)

Source: own elaboration in Workbench (Sciamble Corp., 2021)
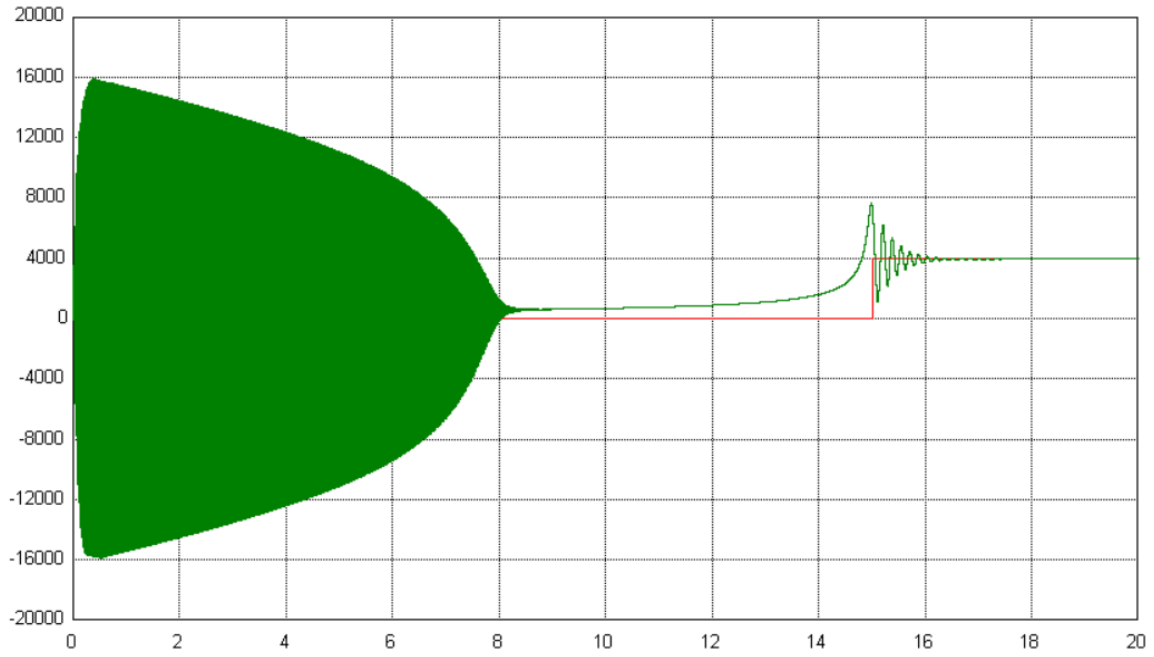
Figure 24. Electromagnetic and load torque (step in load torque of 25% rated torque)

Source: own elaboration in Workbench (Sciamble Corp., 2021)
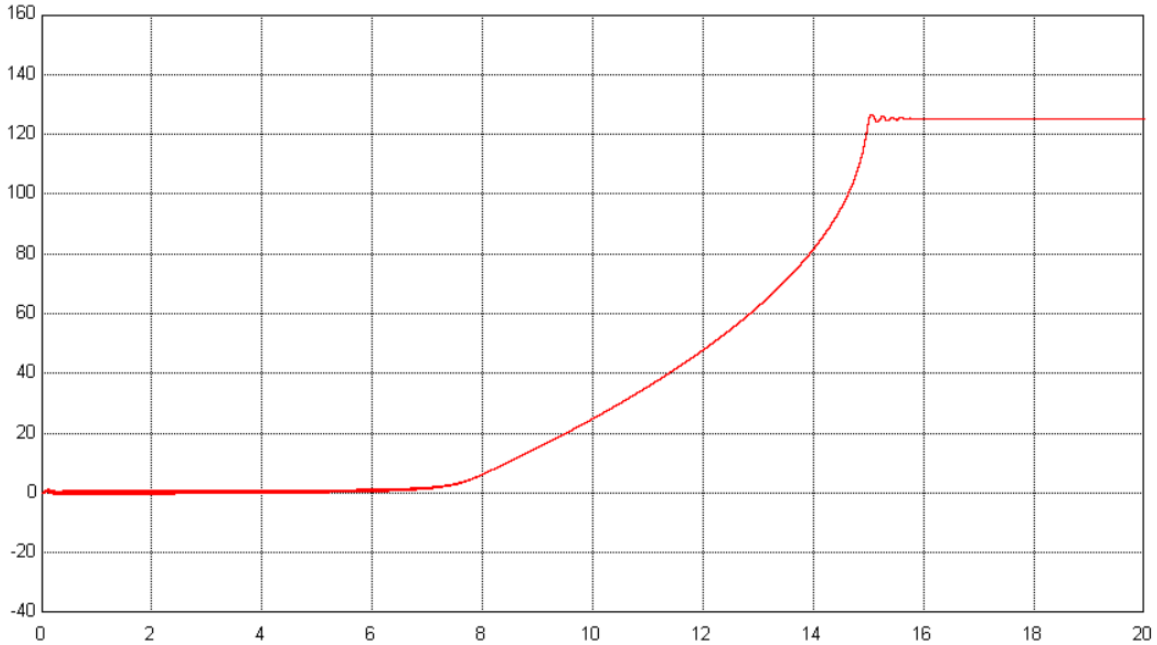
Figure 25. Mechanical speed (step in load torque of 25% rated torque)

Source: own elaboration in Workbench (Sciamble Corp., 2021)

It can be observed how a time interval is necessary for the different variables to settle down properly. Although both the currents and electromagnetic torque need around 8-10 seconds, the mechanical speed requires 15 seconds to settle. That is why the simulation time is 20 seconds and the load torque step time has been selected at 15 seconds.

In the settling interval, the three-phase currents are overlapped, with a separation of 120°. During the first seconds of the simulation, both rotor and stator experience a high intensity amplitude, which will decrease as the electromagnetic torque's amplitude decreases (as it can be checked in Eq. B-9 in Appendix B, the torque is directly proportional to the currents). When the step change in load torque occurs, these variables will also need a short period of time to settle again.

The mechanical speed progressively increases until it reaches 124.4 rad/s, which is $\omega_{mech} = \frac{2}{p} * \omega_m$, where ω_m is the rotor speed in electrical rad/s. In this simulation, the reference speed was chosen to be the mechanical speed. Independently of the reference speed chosen, the system will always settle at the mechanical speed. The electromagnetic torque closely follows the load torque once the speed is constant.

5.4 Computation of initial values

As it has been previously discussed in chapter 2, one of the main advantages of using DFIGs is that they do not always need to be operating at full rated conditions. In this section, we will calculate the steady state values of the torque, relative speeds, and voltages, currents, and fluxes of both the stator and rotor. This will be done under rated conditions and at 50% of rated torque.

We will align the *dq* frame with the stator flux linkage space vector, as we explained in section 4.3.

5.4.1 Calculations in *dq* reference frame at rated parameters

    a. Electromagnetic torque

$$T_{em} = T_{rated} = 15.9 \ kNm$$

    b. Stator and rotor flux linkage speeds

$$\omega_{da} = 0 \ rad/s$$

$$\omega_{dA} = \omega_{da} - \frac{P}{2}\omega_{mech}$$

    c. Stator and rotor voltages

$$\begin{bmatrix} v_{sd} \\ v_{sq} \\ v_{rd} \\ v_{rq} \end{bmatrix} = \begin{bmatrix} 5.17 \\ 689.98 \\ 0 \\ 0 \end{bmatrix} [V]$$

    d. Stator and rotor currents

$$\begin{bmatrix} i_{sd} \\ i_{sq} \\ i_{rd} \\ i_{rq} \end{bmatrix} = \begin{bmatrix} 2586.86 \\ 2929.43 \\ -1941.75 \\ -3090.23 \end{bmatrix} [A]$$

    e. Stator and rotor flux linkages

$$\begin{bmatrix} \lambda_{sd} \\ \lambda_{sq} \\ \lambda_{rd} \\ \lambda_{rq} \end{bmatrix} = \begin{bmatrix} 1.81 \\ 0 \\ 1.23 \\ -0.77 \end{bmatrix} [Wb]$$

5.4.2   Calculations in *dq* reference frame at rated voltage and 50% of rated torque

Once the rated torque has changed, so will the slip. Following Eq. 5-1, that relates torque to slip speed (Casadei et al., 2006), a further simplification can be made if the slip value is very low (assuming $\omega_{slip} * L'_{lr} = 0$), resulting in Eq. 5-2,

$$T_{em} = 3 * R'_r * \frac{V_{rms}^2}{\omega_{syn}^2} * \frac{\omega_{slip}}{R'^2_r + (\frac{P}{2} * \omega_{slip} * L'_{lr})^2} \tag{5-1}$$

$$T_{em} = 3 * \frac{V_{rms}^2}{\omega_{syn}^2} * \frac{\omega_{slip}}{R'_r} \tag{5-2}$$

Therefore,

$$\omega_{slip} = 1.414 \; rad/s$$

$$s = \frac{\omega_{slip}}{\omega_{syn}} = 0.00375$$

a. Electromagnetic torque

$$T_{em} = \frac{1}{2} * T_{rated} = 7.95 \; kNm$$

b. Stator and rotor flux linkage speeds

$$\omega_{da} = 0 \; rad/s$$

$$\omega_{dA} = \omega_{da} - \frac{P}{2}\omega_{mech}$$

c. Stator and rotor voltages

61

$$\begin{bmatrix} v_{sd} \\ v_{sq} \\ v_{rd} \\ v_{rq} \end{bmatrix} = \begin{bmatrix} 2.19 \\ 690 \\ 0 \\ 0 \end{bmatrix} [V]$$

d. Stator and rotor currents

$$\begin{bmatrix} i_{sd} \\ i_{sq} \\ i_{rd} \\ i_{rq} \end{bmatrix} = \begin{bmatrix} 1097.53 \\ 1453.45 \\ -362.39 \\ -1537.95 \end{bmatrix} [A]$$

e. Stator and rotor flux linkages

$$\begin{bmatrix} \lambda_{sd} \\ \lambda_{sq} \\ \lambda_{rd} \\ \lambda_{rq} \end{bmatrix} = \begin{bmatrix} 1.82 \\ 0 \\ 1.63 \\ -0.38 \end{bmatrix} [Wb]$$

5.4.3 Steady state initialization values verification

We need to properly initialize all the integrators in the latter sections of this chapter, where we will implement a controller and simulate the motor at rated conditions. In this section, we will check if the steady state values that have been found in section 5.4.1 are correct.

The steady state values do not need a long simulation time, therefore the simulation will last 2 seconds. If the initialization values and the initial voltage are correct, then the electromagnetic torque and the mechanical speed should be straight lines at the computed value. Otherwise, it will fluctuate initially and settle down.
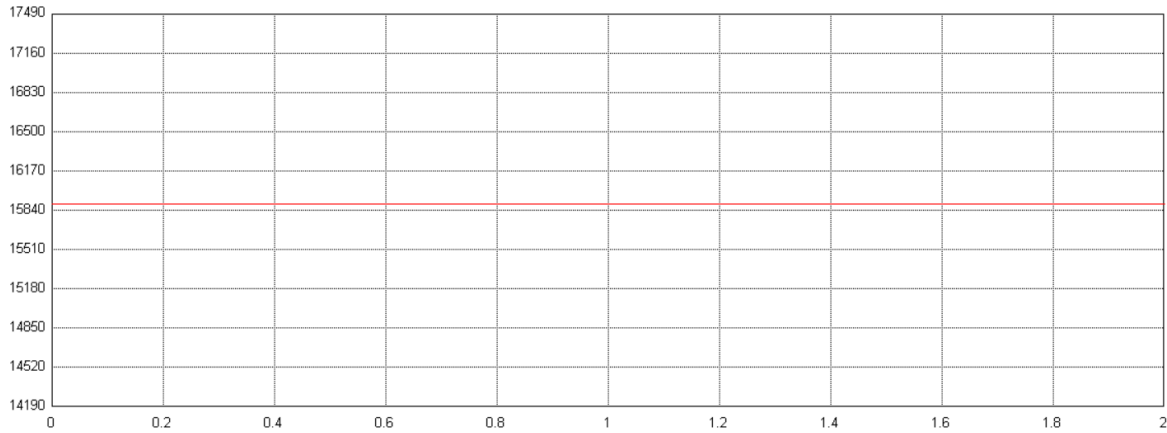
Figure 26. Initialization check for the electromagnetic torque

Source: own elaboration in Workbench (Sciamble Corp., 2021)
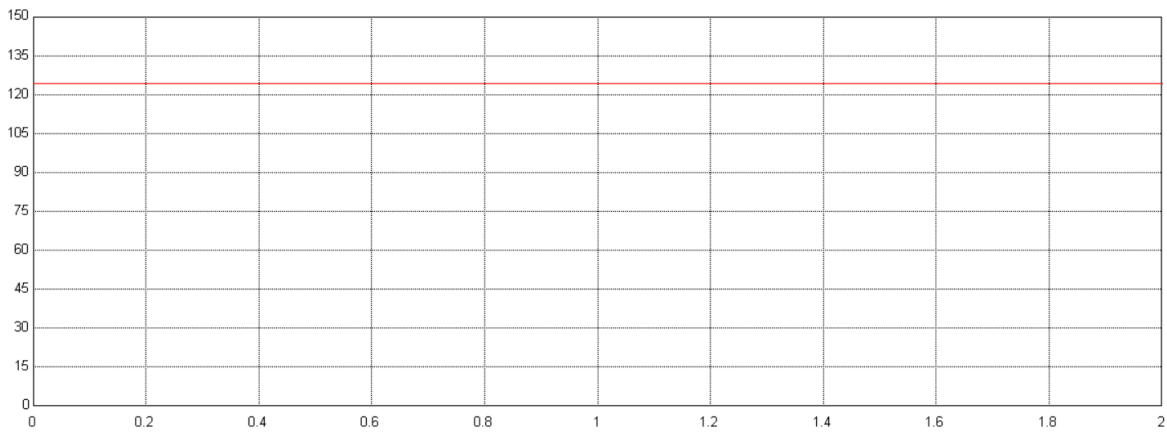
Figure 27. Initialization check for the mechanical speed

Source: own elaboration in Workbench (Sciamble Corp., 2021)

Figs. 26 and 27 show that both values are constant and at their expected values (15.9 kNm for the torque and 126.9 rad/s for the speed).

This method of initialization is very crucial in numerical simulations. To achieve robust yet fast convergence in our solver, from the practical point of view, the initial conditions that have been calculated are first used as the initial conditions. This way, if we are operating with more complicated models, which will take more time and memory to simulate, convergence will occur faster than if we were simulating from zero steady state conditions (Pandey and Pileggi, 2019).

5.5 PI controller modeling

As it has been studied in Chapter 4.3, we are going to build two different controllers: one for rotor current and another one for rotor speed. Appropriate bandwidth speed and phase margin should be selected for both loops.

Two different inner current loops will be modelled, for the rotor d- and q-axes. Both transfer function will turn up to be the same. They are obtained from Eqs. 4-12 and 4-13 in section 4.3.1,

$$\frac{i_{rd}}{v_{rd}} = \frac{1}{R_r + s\sigma L_r} \tag{5-3}$$

$$\frac{i_{rq}}{v_{rq}} = \frac{1}{R_r + s\sigma L_r} \tag{5-4}$$

In addition, we will add an outer speed loop. Its transfer function, from Eq. 4-14 in section 4.3.2,

$$\frac{T_{em}}{i_{rq}} = k_t = -\frac{p}{2} * \frac{L_m}{L_s} * \lambda_{sd} \tag{5-5}$$

The speed controller bandwidth is chosen as 10 rad/s, because it is a value that makes sense after trying different possibilities during simulations. The settling time of the system is reasonable with the initial values. A 10x scaling of the inner current loop seems insufficient for this motor, hence choosing a higher bandwidth of 20x for inner current loop, 200 rad/s.

The phase margin is chosen at 60° because it provides a moderately fast response and involves little energy in transients (Mahvash, 2019).

Figs. 28 and 29 represent the PI models that will be implemented in the motor model in the next section. The gain values are obtained by following the procedure on Sciamble's website (https://sciamble.com/resources/pe-drives-lab/advanced-drives/im-vector-control, last accessed June 6, 2022):

- Outer speed loop PI gain values

$$k_p = -117.82$$

$$k_i = -680.26$$

- Inner current loop PI gain values

$$k_{pi} = 0.04$$

$$k_{ii} = 5.26$$
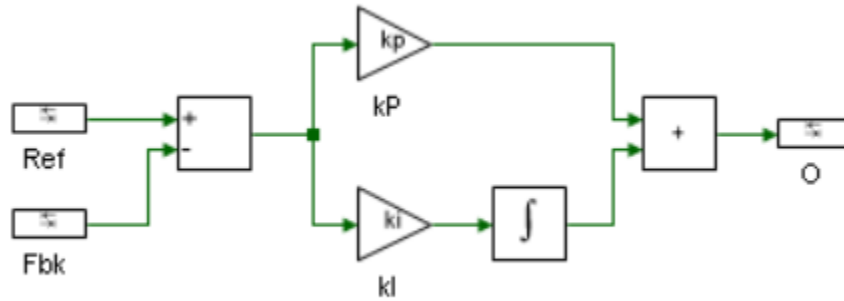
Figure 28. Speed PI controller

Source: own elaboration in Workbench (Sciamble Corp., 2021)
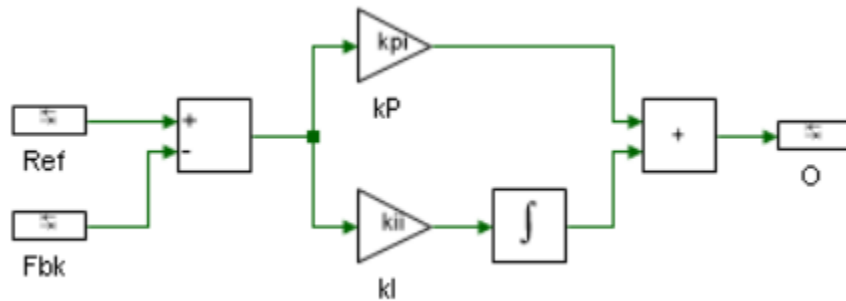
Figure 29. Stator and rotor current PI controllers

Source: own elaboration in Workbench (Sciamble Corp., 2021)

5.6 DFIG analysis in motoring mode

The controller that has been previously described will be added to our DFIG model. Therefore, an estimator model will be included in the Workbench model. We will use a rotor position estimator, as it has been studied in chapter 4 of this project. It will estimate the stator flux linkage space vector λ_{sd} and the stator flux linkage speed ω_{da}. With ω_{da}, the rotor flux linkage space vector angle θ_{dA} can be found. Using the appropriate *abc* into *dq* conversion subsystems, the rotor current can be

calculated and sent as feedback to the system. Details of the model and estimator can be found in Figs. 30-32.

It will be key that all the integrators of the system are correctly initialized with the values that have been calculated in section 5.4 of the project.
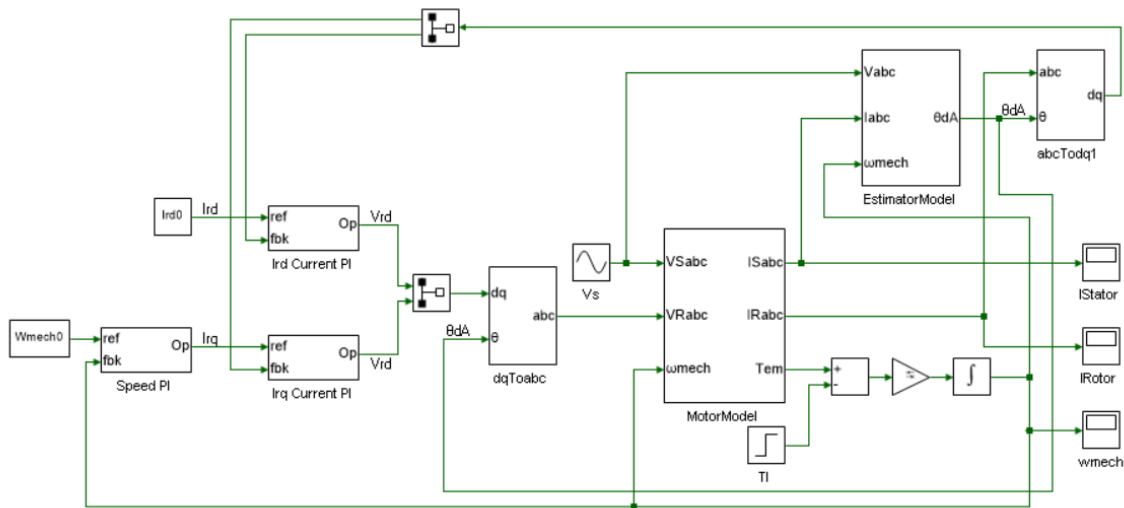
Figure 30. DFIG model

Source: own elaboration in Workbench (Sciamble Corp., 2021)
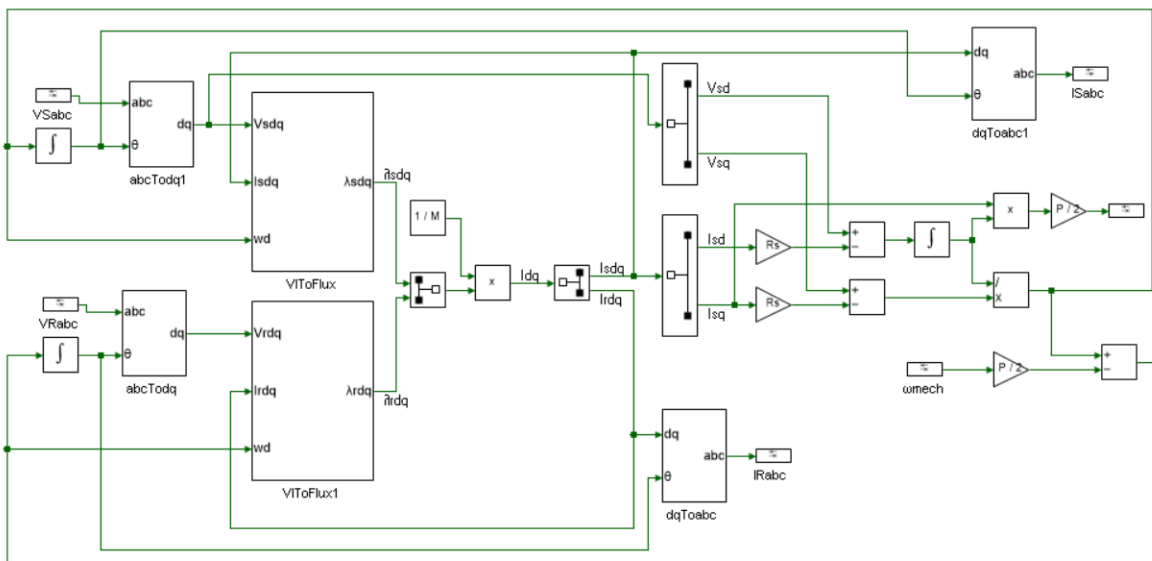
Figure 31. Motor model

Source: own elaboration in Workbench (Sciamble Corp., 2021)

66
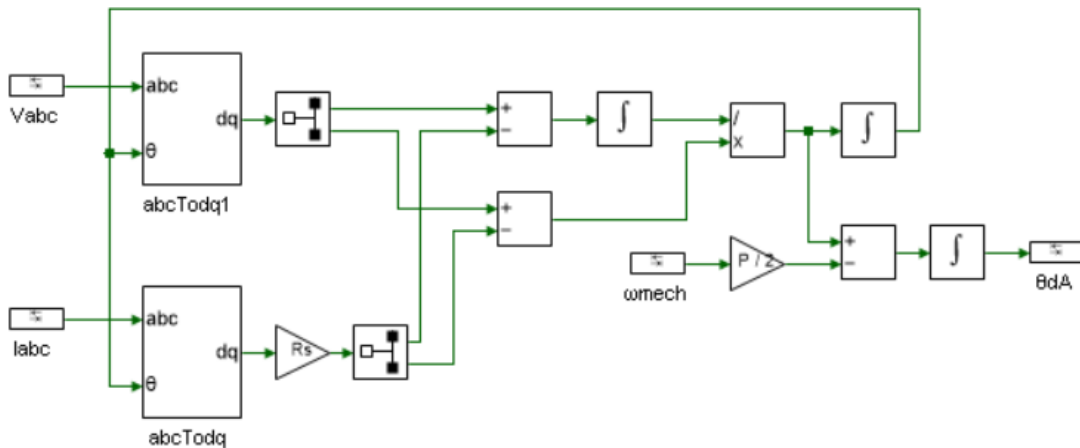
Figure 32. Estimator model

Source: own elaboration in Workbench (Sciamble Corp., 2021)

For the simulation of the motor, we are going to study how different variables behave when a step change in torque occurs, at 50% of its rated torque at t = 1 s. The simulation time shall be 4 seconds, found after different simulations, such so that we can observe the variables once they are settled. Step time has been chosen 0.1 ms, small enough to run the simulation in fractions of a second, and big enough to show correct output graphs in the scopes.

Fig. 33 shows the stator currents and Fig. 34, the rotor currents. Note that color red refers to *a*-phase; green, *b*-phase; and blue, *c*-phase. The mechanical speed is displayed in Fig. 35. Appendix C gathers the script code that is being used in the simulation.

The analysis of this simulation will be done in the next section, so that it is possible to compare the results with the motor in generating mode.

Figure 33. Stator currents (step in load torque of 50% rated torque). Motoring mode

Source: own elaboration in Workbench (Sciamble Corp., 2021)

Figure 34. Rotor currents (step in load torque of 50% rated torque). Motoring mode

Source: own elaboration in Workbench (Sciamble Corp., 2021)

Figure 35. Mechanical speed (step in load torque of 50% rated torque). Motoring mode

Source: own elaboration in Workbench (Sciamble Corp., 2021)

5.7 DFIG analysis in generating mode

This final section studies what differs if the motor operates in generating mode instead of motoring mode (i.e., the rated slip changes from positive $s = 0.01$ to negative $s = -0.01$). The simulation script for this scenario is the same as the one in Appendix C, but changing the rated slip to the negative value. Same graphic results will be presented as before: stator and rotor currents in Figs. 36 and 37, and the mechanical speed in Fig. 38. Lastly, a comparison between both operating modes will be done.
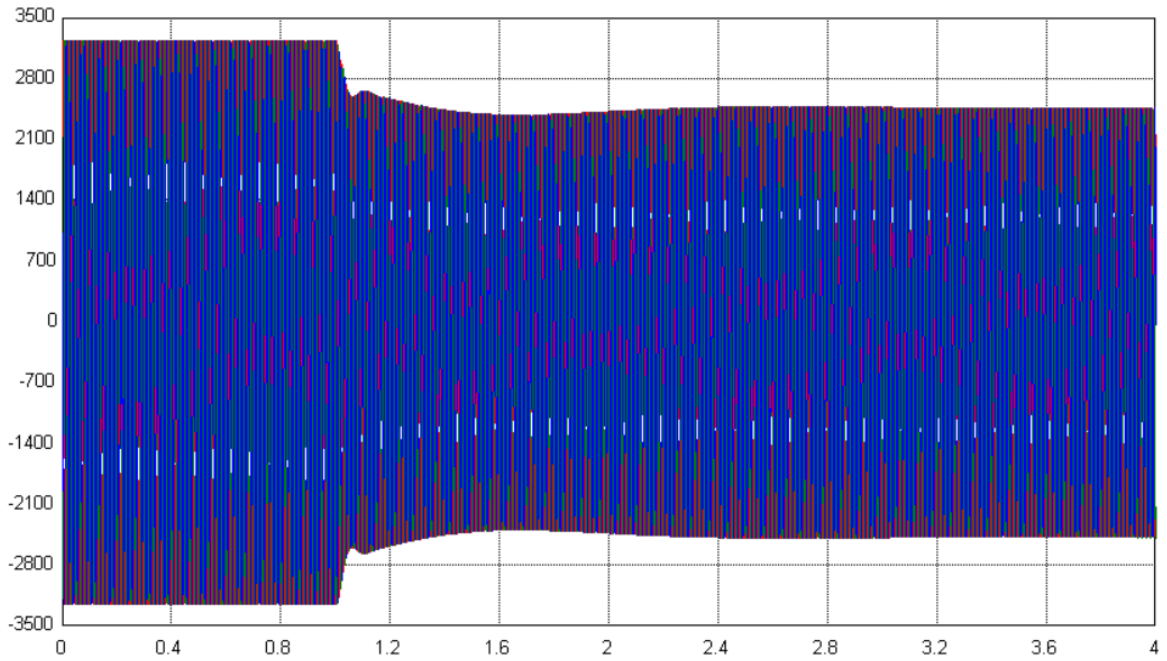
Figure 36. Stator currents (step in load torque of 50% rated torque). Generating mode

Source: own elaboration in Workbench (Sciamble Corp., 2021)
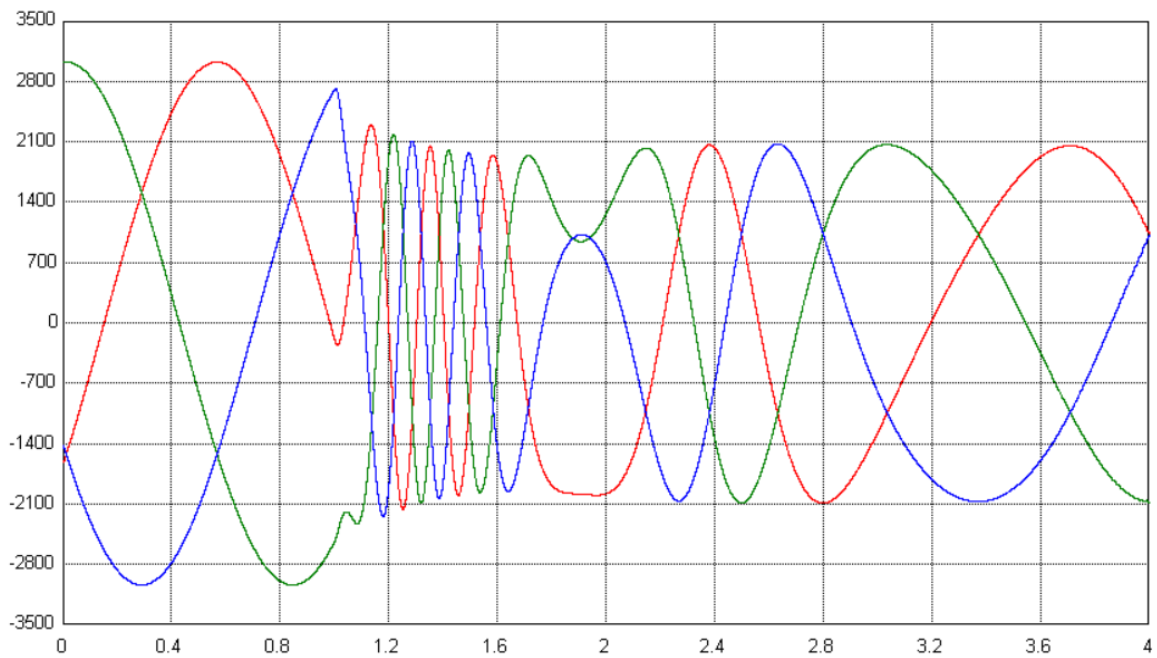
Figure 37. Rotor currents (step in load torque of 50% rated torque). Generating mode
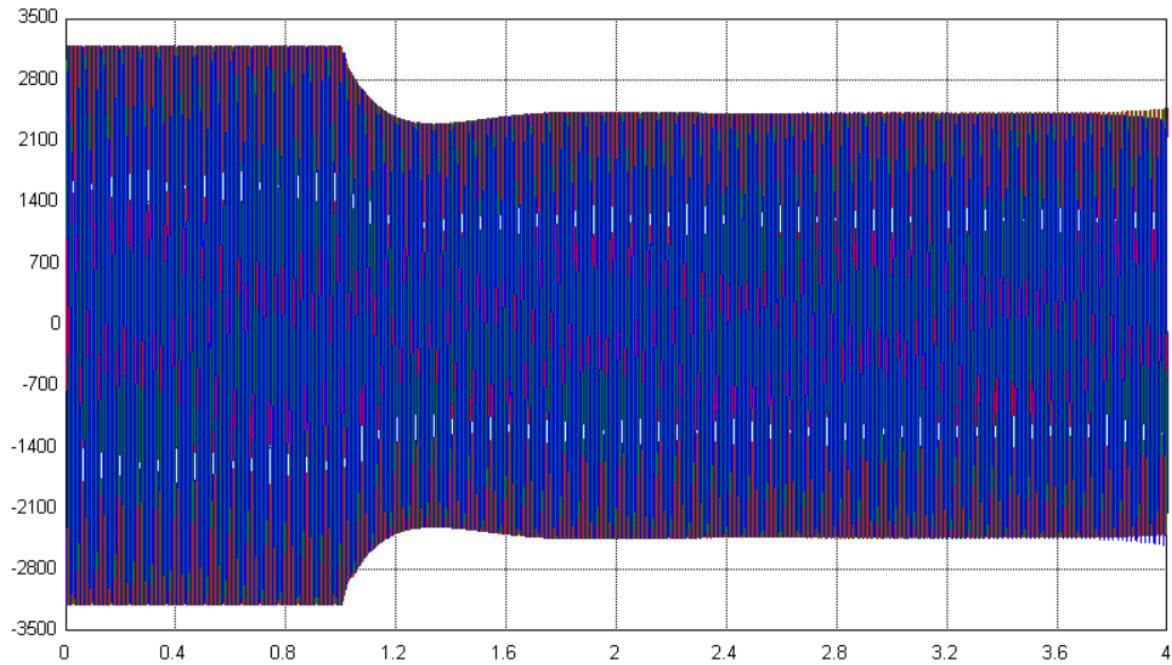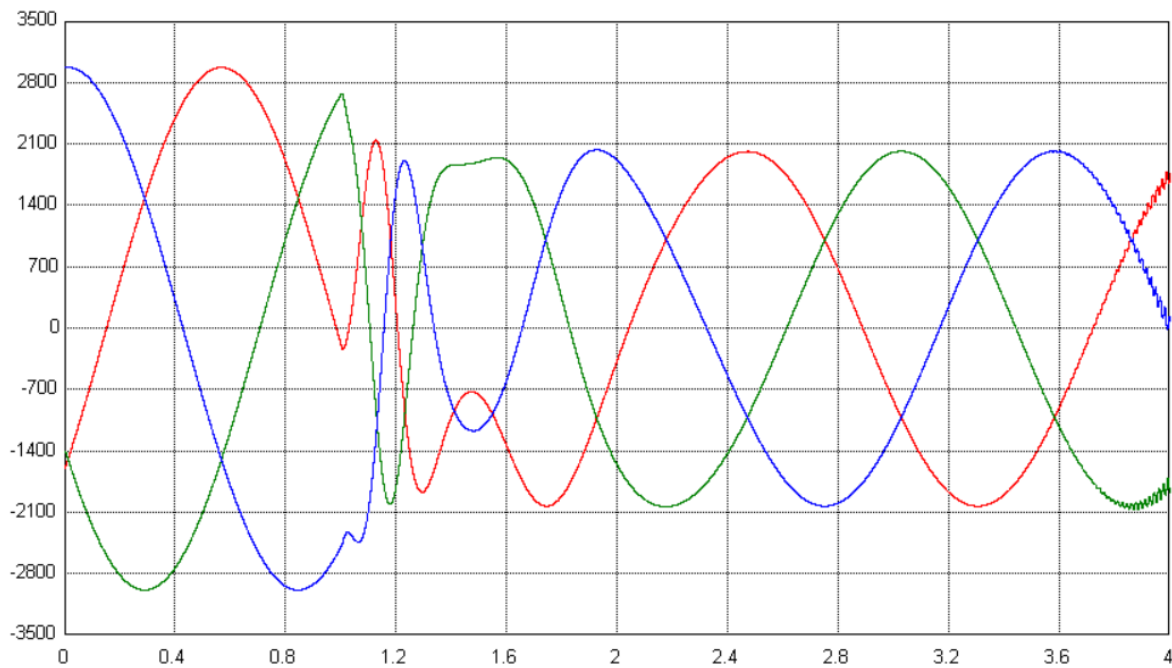
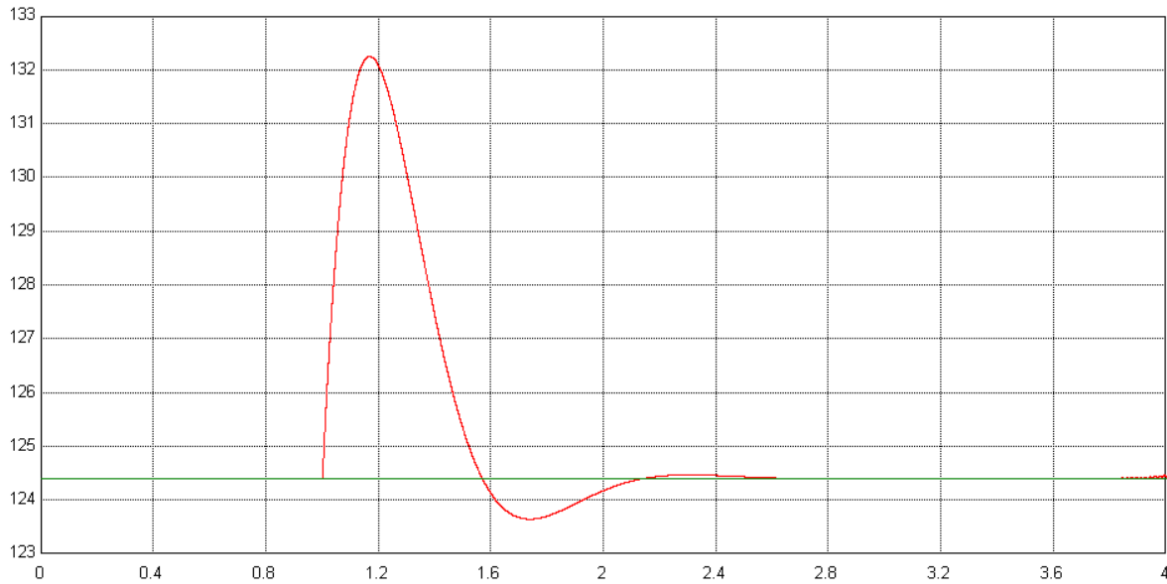*Source: own elaboration in Workbench (Sciamble Corp., 2021)*
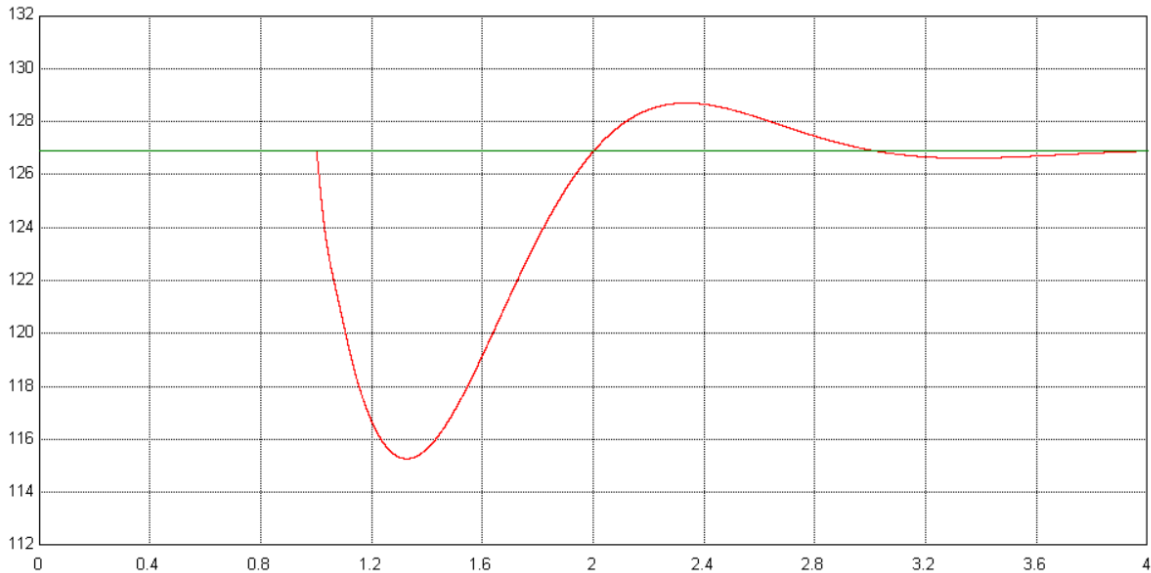
Figure 38. Mechanical speed (step in load torque of 50% rated torque). Generating mode

Source: own elaboration in Workbench (Sciamble Corp., 2021)

We are going to use the computations made in subsection 5.3.1 to analyze the results that have been obtained. Firstly, it can clearly be observed how all the currents are at steady values until the step load torque is applied. The steady state values perfectly match the ones that were calculated previously: 3185.47 A and 2979.92 A for stator and rotor currents, respectively.

The stator current has a smaller period than the rotor current, to be precise, 100 times smaller, as it is rotating at the electrical frequency (376.99 rad/s) while the rotor current is rotating at the rotor frequency, which is $\omega_r = s * \omega_e = 3.77 \ rad/s$.

Both currents are three-phase, sinusoidally distributed waves separated 120°. Stator currents need less time than rotor currents to reach stability. However, there is a key aspect when comparing rotor currents of both modes in Figs. 34 and 37: their phase sequence is inverted, meaning the a-phase (red) is the same, but b- (green) and c-phases (blue) are swapped. This is because the rotor currents rotate at $\omega_r = s * \omega_e$. Therefore, when the slip is positive (motoring mode), the speed will be +3.77 rad/s; and when it is negative (generating), -3.77 rad/s.

Lastly, it can also be observed how the mechanical speed reaches different values. This makes sense, as it depends on the slip. At a positive rated slip, the mechanical speed tends to a speed smaller than the synchronous speed ($\omega_m = (1 - s) * \omega_{sync} = 124.4$ rad/s); and at negative slip, $\omega_m = 126.9 \ rad/s$ is bigger than the electrical frequency.

6. CONCLUDING REMARKS

Sustainable energy sources are a reality. Wind energy is going to be fundamental for the decarbonization of our economy. We are experiencing a new world where technologies continuously improve, reducing their costs and improving their performance.

The purpose of this work has been to understand how the implementation of doubly-fed induction generators can shape our future, going through a thorough study of how they work, their advantages and disadvantages compared to other wind turbine trends, and finally modeling and simulating a DFIG to see its behavior. We applied the knowledge acquired in the fields of control and dynamic systems, power systems, electric machines, and electric drives.

Starting with an induction motor of typical values, we calculated its different variables using the per-phase equivalent circuit. We obtained stator and rotor currents, induced rotor voltages, space vector's rotating speed, electromagnetic torque, and the power balance of the motor, obtaining an efficiency of 97.5%. We simulated the model's response to a step change in torque of 25% of rated torque, studying how the system stabilized after some seconds at our expected values.

Afterwards, the vector control of the motor was done, implementing the adequate power electronics interface. This included a rotor position estimator and two PI controllers, which were also modeled. All the integrators were initialized with the appropriate values for the simulating conditions. The model was simulated at rated voltage and 50% of rated torque, as a motor and as a generator. We focused on the study of the currents and the mechanical speed. Lastly, we compared both simulating modes and analyzed the results.

As it had been expected, the rotor and stator currents both matched the values that had been calculated using the equivalent circuit. It was most interesting studying how the sinusoidal waves behaved, and how the speed their space vectors rotated differed as it had been predicted.

We verified that the mechanical speed followed the pair of poles relation (three times smaller than the electrical frequency), with the slip factor. Therefore, when acting in motoring speed, the mechanical speed was 124.4 rad/s; and in motoring mode, 126.9 rad/s. These values needed a couple of seconds of settling time and were equal to what we had calculated previously.

This project is limited by the simulating world. Although we were able to model and simulate DFIGs in a computer program, having understood the engineering behind them, it would be of the most notable interest to study DFIGs in the real world.

Hence, a possible extension for this work is simulating these turbine generators in real windmills. Although it would require large amounts of money and time, it would be the ideal way of checking this project's results. As typical values were provided for the induction motor, instead of having to build a new turbine following these parameters, it would be simpler to repeat the calculations and simulations for an already existing DFIG.

Further extensions for this project could include a more thorough motor analysis, with no simplified circuit and acknowledging all parasitics. A different *dq* frame alignment could also be chosen, and the motor could even be simulated in the three-phase frame. However, these calculations would only complicate the model and equations used, requiring more computational power in order to arrive to identical conclusions.

Regarding the estimator model, as it was explained in chapter 4, a low pass filter could be added to correct any accumulation of offset, avoiding any non-converging results. This has not been the case of our simulation, but it would be a good error prevention method. Instead of using the rotor position estimator that has been described, we could have created a MRAS estimator, as it was described in chapter 3, which would be more complete as it would estimate the mechanical speed and the rotor flux linkage space vector.

It will surely be attractive to see how future alternatives, such as brushless DFIGs will be implemented in the years to come. There still is a lot of research to be done while at the same time, the future begins to look more promising.

REFERENCES

Articles and books

Ban, D., Žarko, D., Mađerčić, M., Zagreb, K., Croatia, Z., Čulig, M. & Petrinić. (2022). Generator Technology for Wind Turbines, Trends in Application and Production in Croatia.

Brekken, T. (2005). A novel control scheme for a doubly-fed wind generator under unbalanced grid voltage conditions. PhD thesis. University of Minnesota.

Brune C.S., Spee, R. & Wallace, A.K. (1994). Experimental evaluation of a variable speed, doubly-fed wind-power generation system. IEEE Trans. on Industry Applications, pp. 648 – 655.

Butterfield, C.P., Hansen, A.C., Simms, D. & Scott, G. (1991). Dynamic Stall Wind Turbine Blades.

Carrasco, J.M., Franquelo, L., Bialasiewicz, J., Galvan, E., Portillo, R., Prats, M.M., Leon, J. & Moreno-Alfonso, N. (2006). Power-Electronic Systems for the Grid Integration of Renewable Energy Sources: A Survey. Industrial Electronics, IEEE Transactions on. 53. 1002 - 1016. 10.1109/TIE.2006.878356.

Casadei, D., Serra, G., Tani, A., & Zarri, L. (2006). Assessment of direct torque control for induction motor drives. Bulletin of The Polish Academy of Sciences-technical Sciences, 54, 237-254.

Clark, K., Miller, N. & Sanchez-Gasca, J. (2010). Modeling of GE Wind Turbine-Generators for Grid Studies.

Diepeveen, N. (2013). "On Fluid Power Transmission for Offshore Wind Turbines", PhD thesis Delft University of Technology.

Endale, S.M. & Tuka, M.B. (2021). Fault Ride through Capability Analysis of Wind Turbine with Doubly-fed Induction Generator.

Holtz, J. (2002). Sensorless control of induction motor drives. Proceedings of the IEEE 90 (8): 1359–1394.

Höhn, B.-R. (2011). Future transmissions for wind turbines. Applied Mechanics and Materials (vol. 86), pp.18-25.

Lewis, C. & Muller, J. (2007). A direct drive wind turbine HTS generator. IEEE Power Engineering Society General Meeting, pp. 1-8.

Long, T., Shao, S., Abdi, E., Malliband, P., Mathekga, M.E., McMahon, R.A. & Tavner, P.J. (2012). Symmetrical low voltage ride-through of a 250 kW Brushless DFIG. 6th IET Int. Conf. on Power Electronics, Machines and Drives (PEMD).

Mahvash, H., Taher, S.A., Rahimi, M., & Shahidehpour, M. (2019). Enhancement of DFIG performance at high wind speed using fractional order PI controller in pitch compensation loop. International Journal of Electrical Power & Energy Systems.

Mohan N. & Raju S. (2021). Analysis and Control of Electric Drives: Simulations and Laboratory Implementation.

Okedu, K.E. & Barghash, H.F.A. (2021). Enhancing the Performance of DFIG Wind Turbines Considering Excitation Parameters of the Insulated Gate Bipolar Transistors and a New PLL Scheme.

Ozsoy, E., Golubovic, E., Sabanovic, A., Bogosyan, S. & Gokasan, M. (2014). Modeling and control of doubly-fed induction generator with a disturbance observer: A stator voltage oriented approach. Turkish Journal of Electrical Engineering and Computer Sciences. 24. 10.3906/elk-1312-104.

Pandey A. & Pileggi L. (2019). Steady-State Simulation for Combined Transmission and Distribution Systems

Parida A. & Chatterjee D. (2014). A robust parameter non-sensitive rotor position and speed estimator for DFIG.

Phan, T., Nguyen, V., Hossain, M., To, A., Tran, H. & Phan, N. (2016). Transient Responses of the Doubly-Fed Induction Generator Wind Turbine under Grid Fault Conditions.

Polinder, H., Ferreira, J., Jensen, B., Abrahamsen, A., Atallah, K. & Mcmahon, R. (2013). Trends in Wind Turbine Generator Systems. IEEE Journal of Emerging and Selected Topics in Power Electronics. 1. 174-185. 10.1109/JESTPE.2013.2280428.

Rens, J., Atallah, K., Calverley, S.D. & Howe, D. (2010). A novel magnetic harmonic gear. IEEE Trans. on Industry Applications, pp. 206-212.

Rossi, C., Corbelli, P. & Grandi, G. (2009). W-CVT continuously variable transmission for wind energy conversion system, in Proc. of the IEEE conference on power electronics and machines in wind applications, pp. 1-10.

Smajo, J., Smajo, M. & Vukadinovic, D. (2005). Reference Value Choice of the Wind Turbine Active Power with Doubly-Fed Induction Generator.

Snitchler, G., Gamble, B., King, C. & Winn, P. (2011). 10 MW class superconductor wind turbine generators. IEEE Trans. on Applied Superconductivity, pp. 1089-1092.

Staton, D., Deodhar, R., Soong, W.L. & Miller, T.J.E. (1996). Torque prediction using the flux-MMF diagram in AC, DC, and reluctance motors. Industry Applications, IEEE Transactions on. 32. 180 - 188. 10.1109/28.485830.

Tewari, S., Geyer, C.J., and Mohan, N. (2011). A statistical model for wind power forecast error and its application to the estimation of penalties in liberalized markets. IEEE Transactions on Power Systems 26 (4).

Wessels, C., Gebhart, F. & Fuchs, R.W. (2011). Fault ride-through of a DFIG wind turbine using a dynamic voltage restorer during symmetrical and asymmetrical grid faults. IEEE Trans. on Power Electronics, pp. 807-815.

Programs

Sciamble Corp. (2021). *Workbench*. Developed by Siddharth Raju at the University of Minnesota. Available online at: https://sciamble.com/, last checked June 6, 2022.

APPENDIX A: BRIEF OVERVIEW OF INDUCTION MOTOR THEORY

A.1   Structure of an induction motor

The IM stator is the same as that of the Permanent Magnet AC (PMAC) motor stator. It has sinusoidally distributed windings for each of the phases. The rotor instead of being made of permanent magnets, is conformed of equally spaced copper or aluminum bars shorted together. The copper bars are inserted into slots made in laminated Silicon or iron plates, which provide the least reluctance path for the flux.

A.2   Rotor sinusoidal current distribution

In the stator, sinusoidal current distribution is present. Therefore, sinusoidal flux distribution is obtained by sinusoidally varying the number of conductors per slot per phase. As the 3-phase currents vary in time, the sinusoidal flux distribution in the airgap rotates at the same frequency as the phase currents.

In the case of a PMAC motor, a sinusoidal rotor flux distribution is obtained by appropriately shaping the rotor magnets. On the contrary, in the case of an IM, the current distributes itself sinusoidally due to the laws of induction. Unlike the stator, each slot of the rotor has the same number of conductors (one), and each of these conductors are of the same thickness, length, etc.

Let's begin with the case where the rotor speed is zero. Let the stator voltage frequency be ω_e, which in turn is the speed at which the flux due to the stator current (B_{ms}) rotates (for a 2-pole IM). At time $t = t_0$, let B_{ms} space vector be at an angle α with respect to the x-axis. Consider any two diametrically opposite copper bar, forming a loop, at an angle β.

The flux linking the highlighted rotor loop is given by:

$$\emptyset_{loop} = \int_{\beta}^{\beta+2\pi/p} B_{ms}(\theta) * l * r * d\theta = \int_{\beta}^{\beta+2\pi/p} B_{ms,pk} * cos(\alpha - \theta) * l * r * d\theta \qquad \text{(A-1)}$$

$$\emptyset_{loop} = \frac{4}{p} * l * r * B_{ms,pk} * \sin{(\alpha - \beta)} \qquad \text{(A-2)}$$

where:

- p is the number of pair of poles
- l is the length of the induction motor
- r is the radius of the induction motor

- $B_{ms,pk}$ is the peak value of the stator current flux
- α is the angle of the stator current flux vector with respect to the a-phase magnetic axis
- β is the angle at which the loop is being formed with respect to the a-phase magnetic axis
- θ is the angle at any moment t

The electromagnetic force (emf) across the highlighted rotor loop is:

$$e_{loop} = N * \frac{d\emptyset}{dt} = \frac{4}{p} * l * r * B_{ms,pk} * \cos{(\alpha - \beta)} * \frac{d\alpha}{dt} \qquad \text{(A-3)}$$

where $\frac{d\alpha}{dt}$ is the speed at which B_{ms} is rotating (ω_e).

We can also express α as $\omega_e t$. Consequently,

$$e_{loop} = 2 * l * r * B_{ms,pk} * \omega_{sync} * \cos{(\omega_e * t - \beta)} \qquad \text{(A-4)}$$

where:

- ω_{sync} is the synchronous speed of the motor
- ω_e is the electrical speed of the motor

Firstly, by fixing the B_{ms} space vector position (as α is constant), means that when going around the rotor, each conductor's loop voltage varies sinusoidally in space as β varies from 0 to π. Secondly, for a given rotor conductor loop (β is constant), as the induced stator current across the airgap flux density rotates, the emf on the rotor varies sinusoidally in time as α varies from 0 to 2π. Thirdly, emf is maximum for the conductor along the direction where the B_{ms} space vector is maximum (α = β). At this orientation, flux linking the loop is zero. In fact, emf is not proportional to the flux but to the derivative of the flux respect to time.

As the B_{ms} space vector rotates in space at the synchronous speed, the voltage across the copper bar varies sinusoidally. Since all bars are made of the same material and have the same dimensions, and the voltages on a bar with a 180° offset are of the same magnitude but opposite polarity, the current through each bar is, through superposition,

$$i(\beta) = \frac{e(\beta)}{R_{bar}} = \frac{l * r}{R_{bar}} * B_{ms,pk} * \omega_{sync} * \cos{(\omega_e * t - \beta)} \qquad \text{(A-5)}$$

where R_{bar} is the resistance of the bar.

It should not be forgotten that so far, we have only considered the case where the rotor is at a standstill. Despite this fact, the rotor current space vector rotates at the synchronous speed due to the $\omega_{sync} * t$ term in the previous equation.

A.3   Rotor flux

For this analysis, the stator resistance R_s, stator and rotor leakage inductances L_{ls} and L_{lr} are assumed to be zero.

The current in the rotor will try to establish a flux different from B_{ms}, but like the transformer, where any flux established by the secondary is cancelled out by additional current in the primary, the induction motor stator draws equivalent current to cancel the changing flux current to cancel the changing flux established by the current in the rotor.

Unlike in PMACs, where airgap flux is a combination of both the flux established by the rotor magnet as well as flux due to stator current, in an induction motor, the flux in the airgap is solely due to stator magnetizing currents (I_{ms}).

The stator phase voltage $V_a = V_{pk} * \sin(\omega_e * t)$ determines the magnetizing current I_m, which lags the voltage by 90°,

$$I_m = \frac{V_{pk}}{\omega_e * L_m} * \sin(\omega_e * t - 90°) \tag{A-6}$$

where:

- V_{pk} is the peak value of the stator voltage
- $L_m = \frac{3}{2} * L_{m,1-phase} = \frac{3}{2} * \frac{\pi * \mu_0 * r * l}{l_g} * (\frac{N_s}{p})^2$ refers to the mutual inductance

This I_m establishes B_{ms} which in turn induces voltage in the rotor which lags the B_{ms} by 90°,

$$V_r = l * r * B_{ms,pk} * \omega_{sync} * \sin(\omega_r * t - 180°) \tag{A-7}$$

This leads to a current,

$$I_r = \frac{l * r}{R} * B_{ms,pk} * \omega_{sync} * \sin(\omega_r * t - 180°) \tag{A-8}$$

The current tries to establish additional flux,

$$B_{due\ to\ Ir} = \frac{N_r}{p} * \frac{\mu_0}{l_g} * I_r \qquad\text{(A-9)}$$

where:

- μ_0 is the air gap permeability
- l_g Is the length of the air gap
- N_r represents the equivalent rotor turns: $N_r = \frac{1}{\pi} * N_{rotor-bars}$.

This flux is instantly cancelled out by additional currents drawn by the stator,

$$I'_r = -\frac{N_r}{N_s} * I_r \qquad\text{(A-10)}$$

The stator current is sum of the magnetizing and the reflected rotor current:

$$I_s = I_m + I'_r \qquad\text{(A-11)}$$

The power factor is cos Ø. It is generally preferred to have a power factor as close to one as possible to limit the reactive power. This would require having very low magnetizing current. The magnetizing current itself is determined by the desired flux density in the airgap (typically between 0.65 - 1 T). A smaller air-gap length would ensure higher flux for the same current. In a typical induction motor, at rated operating conditions, the magnetizing current is 10% to 30% of the rated current.

A.4   Electromagnetic torque

The torque produced by a motor with sinusoidal magnetomotive force (mmf) distribution is (Staton et al., 1996),

$$T_{em} = \pi * r * l * \frac{N_s}{2} * B_{pk} * I_{pk} * \sin \delta \qquad\text{(A-12)}$$

where:

- B_{pk} is the rotor flux peak (rotor magnets)
- I_{pk} is the stator current space vector peak
- N_s is the total number of stator turns per phase
- δ is the load angle, angle between flux and current vectors.

The same expression can be derived for an IM with only difference being B_{pk} is the stator flux peak ($B_{ms,pk}$) and I_{pk} is the equivalent reflected rotor current space vector peak ($I'_{r,pk}$). In addition, it must also be noted that δ is now the angle between $B_{ms,pk}$ and $I'_{r,pk}$.

$$T_{em} = \pi * r * l * \frac{N_s}{2} * B_{ms,pk} * I'_{r,pk} * \sin \delta \qquad \text{(A-13)}$$

Next, we are going to compare a permanent magnet synchronous motor (PMSM) with an IM. In the case of a PMSM, the angle between the rotor flux and stator currents (δ) could be controlled by adjusting the angle of the injected current with respect to rotor flux. It is usually preferred to maintain δ = 90° for maximum torque for given current. In contrast, in an IM, the angle between the stator flux and the reflected rotor current is self-determined based on the rotor leakage inductance and cannot be externally controlled.

A.5   Non-zero rotor speed

So far, the analysis has been made for the case where the rotor was at a standstill. All of this holds true when $\omega_m \neq 0$ with one minor modification.

It is apparent that even when $\omega_m = 0$, the rotor will experience a non-zero time-average net torque. This will cause the rotor to rotate, meaning ω_m will not be zero.

PMAC motors cannot be directly started at line frequency because as the B_{ms} vector rotated at line-frequency, the B_r vector was at standstill because the rotor was at standstill and the magnets were not rotating. Since the B_{ms} vector is rotating at relatively high speed, its polarity seen by rotor magnets flips every half cycle before the rotor can catch-up. Thus time-average torque over a cycle is zero.

On the contrary, in an induction motor, since the rotor currents are induced, the rotor current space vector rotates at the same speed as the B_{ms} space vector. Therefore, the time-average torque of a cycle is not zero. This allow for induction motors to be started directly at line frequency.

Consequently, the only modification is in Eq. A-4 derived in section A.2,

$$e_{bar}(\beta) = l * r * B_{ms,pk} * \omega_{slip} * \cos (\omega_r * t - \beta) \qquad \text{(A-14)}$$

where:

- $\omega_{slip} = s * \omega_{sync}$ is the slip frequency

- $\omega_r = s * \omega_e$ is the rotor frequency
- $s = \frac{\omega_{sync} - \omega_m}{\omega_{sync}} = \frac{\omega_{slip}}{\omega_{sync}}$ is the slip
- $\omega_{sync} = \frac{2}{p} * \omega_e$ is the synchronous frequency

A.6   Per-phase steady state equivalent circuit

The per-phase equivalent circuit is represented in Fig. 39. In this subsection, the power analysis of the induction motor will also be done based on the equivalent circuit.
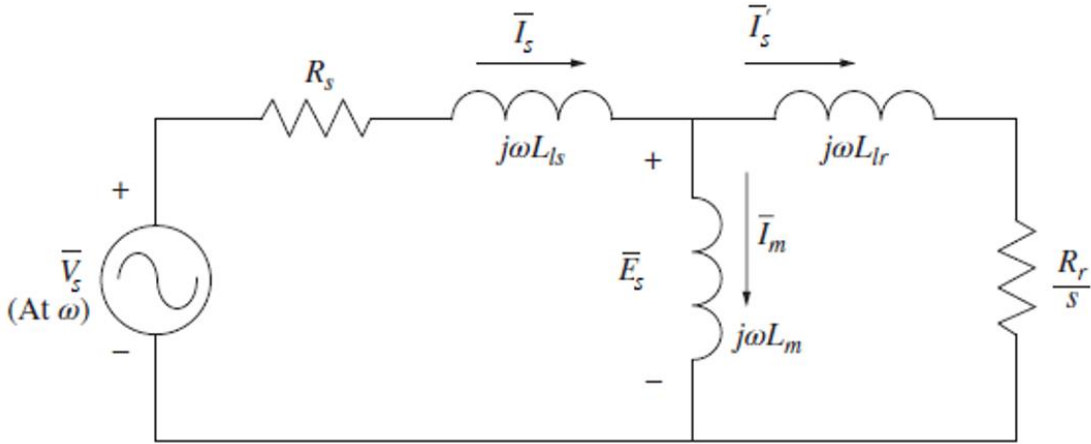
Figure 39. Per-phase equivalent circuit

Source: Mohan and Raju, 2021.

The power lost in the rotor,

$$P_{r,loss} = 3 * I'_{r,rms}{}^2 * R'_r \tag{A-15}$$

The rotor circuit equation (A-16) can be described, and later dividing both sides by s (Eq. A-17),

$$s * E_s = (j * s * \omega_e * L'_{lr} + R'_r) * I'_r \tag{A-16}$$

$$E_s = \left(j * s * \omega_e * L'_{lr} + \frac{R'_r}{s}\right) * I'_r \tag{A-17}$$

The power flowing into the airgap and the power flowing into the mechanical system are described in Eqs. A-18 and A-19, respectively,

$$P_{airgap} = 3 * I'_{r,rms}{}^2 * \frac{R'_r}{s} \qquad \text{(A-18)}$$

$$P_{mech} = T_{em} * \omega_m = P_{airgap} - P_{r,loss} = 3 * I'_{r,rms}{}^2 * R'_r * \left(\frac{1}{s} - 1\right) \qquad \text{(A-19)}$$

In the above equivalent circuit, the $\frac{R'_r}{s}$ term can be split into two components: R'_r and

$R'_r * \left(\frac{1}{s} - 1\right)$. The former represents rotor loss, and the latter represents mechanical power.

APPENDIX B: IM VECTOR CONTROL EQUATIONS

B.1   General equations

Flux linkage equations:

$$\lambda_{sd} = L_s i_{sd} + L_m i_{rd} \tag{B-1}$$

$$\lambda_{sq} = L_s i_{sq} + L_m i_{rq} \tag{B-2}$$

$$\lambda_{rd} = L_m i_{sd} + L_r i_{rd} \tag{B-3}$$

$$\lambda_{rq} = L_m i_{sq} + L_r i_{rq} \tag{B-4}$$

Voltage equations:s

$$V_{sd} = R_s i_{sd} - \omega_{da}\lambda_{sq} + \frac{d\lambda_{sd}}{dt} \tag{B-5}$$

$$V_{sq} = R_s i_{sq} + \omega_{da}\lambda_{sd} + \frac{d\lambda_{sq}}{dt} \tag{B-6}$$

$$V_{rd} = 0 = R_r i_{rd} - \omega_{dA}\lambda_{rq} + \frac{d\lambda_{rd}}{dt} \tag{B-7}$$

$$V_{rq} = 0 = R_r i_{rq} + \omega_{dA}\lambda_{rd} + \frac{d\lambda_{rq}}{dt} \tag{B-8}$$

Mechanical equations:

$$T_{em} = \frac{P}{2}\left(\lambda_{rq} i_{rd} - \lambda_{rd} i_{rq}\right) \tag{B-9}$$

$$\omega_{da} = \omega_m + \omega_{dA} = \frac{P}{2}\omega_{mech} + \omega_{dA} \tag{B-10}$$

B.2 *D*-axis aligned with respect to rotor flux linkage ($\lambda_{rq} = 0$)

From Eq. B-4,

$$i_{rq} = -\frac{L_m}{L_r} i_{sq} \tag{B-11}$$

From Eqs. B-8 and B-11,

$$0 = R_r i_{rq} + \omega_{dA}\lambda_{rd} \Rightarrow$$

$$\omega_{dA} = -\frac{R_r}{\lambda_{rd}} i_{rq} = \frac{R_r}{\lambda_{rd}}\frac{L_m}{L_r} i_{sq} = \frac{L_m}{\tau_r \lambda_{rd}} i_{sq} \tag{B-12}$$

where, τ_r is the rotor time constant $= \frac{L_r}{R_r}$.

From Eqs. B-9 and B-11,

$$T_{em} = -\frac{P}{2}\lambda_{rd}i_{rq} = \frac{P}{2}\frac{L_m}{L_r}\lambda_{rd}i_{sq} \tag{B-13}$$

From Eqs. B-7 and B-3,

$$0 = R_r I_{rd} + \frac{d\lambda_{rd}}{dt} = R_r i_{rd} + \frac{d}{dt}(L_m i_{sd} + L_r i_{rd})$$

$$\Rightarrow 0 = R_r i_{rd}(s) + sL_m i_{sd}(s) + sL_r i_{rd}(s) = (R_r + sL_r)i_{rd}(s) + sL_m i_{sd}(s)$$

$$\Rightarrow i_{rd}(s) = -\frac{sL_m}{sL_r + R_r} i_{sd}(s) \tag{B-14}$$

From Eqs. B-3 and B-14,

$$\lambda_{rd} = L_m i_{sd} + L_r i_{rd}$$

$$\Rightarrow \lambda_{rd}(s) = L_m i_{sd}(s) - \frac{sL_m L_r}{sL_r + R_r} i_{sd}(s) = \frac{L_m R_r}{sL_r + R_r} i_{sd}(s) = \frac{L_m}{s\tau_r + 1} i_{sd}(s) \tag{B-15}$$

85

From Eq. B-3,

$$\lambda_{rd} = L_m i_{sd} + L_r i_{rd}$$

$$\Rightarrow i_{rd} = \frac{\lambda_{rd}}{L_r} - \frac{L_m}{L_r} i_{sd} \tag{B-16}$$

From Eqs. B-1 and B-16,

$$\lambda_{sd} = L_s i_{sd} + L_m i_{rd} = L_s i_{sd} + L_m \left(\frac{\lambda_{rd}}{L_r} - \frac{L_m}{L_r} i_{sd} \right)$$

$$\Rightarrow \lambda_{sd} = L_s \left(1 - \frac{L_m^2}{L_s L_r} \right) i_{sd} + \frac{L_m}{L_r} \lambda_{rd}$$

$$\Rightarrow \lambda_{sd} = L_s \sigma i_{sd} + \frac{L_m}{L_r} \lambda_{rd} \tag{B-17}$$

where, σ is the leakage factor $= \left(1 - \frac{L_m^2}{L_s L_r} \right)$.

From Eqs. B-2 and B-11,

$$\lambda_{sq} = L_s i_{sq} + L_m i_{rq} = L_s i_{sq} - \frac{L_m^2}{L_r} i_{sq} = L_s \left(1 - \frac{L_m^2}{L_s L_r} \right) i_{sq} = \sigma L_s i_{sq} \tag{B-18}$$

From Eqs. B-5, B-17, and B-18,

$$V_{sd} = R_s i_{sd} - \omega_{da} \lambda_{sq} + \frac{d\lambda_{sd}}{dt}$$

$$\Rightarrow V_{sd} = R_s i_{sd} - \omega_{da} \sigma L_s i_{sq} + \frac{d}{dt} \left(L_s \sigma i_{sd} + \frac{L_m}{L_r} \lambda_{rd} \right)$$

$$\Rightarrow V_{sd} = R_s i_{sd} + \sigma L_s \frac{d i_{sd}}{dt} + \frac{L_m}{L_r} \frac{d\lambda_{rd}}{dt} - -\omega_{da} \sigma L_s i_{sq} \tag{B-19}$$

From Eqs. B-6, B-17 and B-18,

$$V_{sq} = R_s i_{sq} + \omega_{da} \lambda_{sd} + \frac{d\lambda_{sq}}{dt}$$

$$\Rightarrow V_{sq} = R_s i_{sq} + \omega_{da} \left(L_s \sigma i_{sd} + \frac{L_m}{L_r} \lambda_{rd} \right) + \frac{d}{dt} \left(\sigma L_s i_{sq} \right)$$

$$\Rightarrow V_{sq} = R_s i_{sq} + \sigma L_s \frac{di_{sq}}{dt} + \omega_{da} \frac{L_m}{L_r} \lambda_{rd} + \omega_{da} \sigma L_s i_{sd} \qquad \text{(B-20)}$$

B.2.1   Ignoring parasitics

Flux linkage equations:

$$\lambda_{sd} = \frac{v_{sq}}{\omega_{da}} = L_m (i_{sd} + i_{rd}) \qquad \text{(B-21)}$$

$$\lambda_{sq} = 0 \qquad \text{(B-22)}$$

$$\lambda_{rd} = \frac{v_{sq}}{\omega_{da}} = L_m (i_{sd} + i_{rd}) \qquad \text{(B-23)}$$

$$\lambda_{rq} = 0 \qquad \text{(B-24)}$$

Voltage equations:

$$V_{sd} = 0 = -\omega_{da} \lambda_{sq} \qquad \text{(B-25)}$$

$$\text{(B-26)}$$
$$V_{sq} = \omega_{da} \lambda_{sd} = \sqrt{\frac{2}{3}} * \widehat{V_s} \equiv constant$$

$$V_{rd} = 0 = -\omega_{dA} \lambda_{rq} \qquad \text{(B-27)}$$

$$V_{rq} = \omega_{dA} \lambda_{rd} = s\, \omega_{dA}\, v_{sq} \qquad \text{(B-28)}$$

where $\widehat{V_s}$ is the amplitude of the stator voltage space vector.

Current equations:

$$i_{sd} = \frac{\lambda_{sd}}{L_m} - i_{rd} = i_{md} - i_{rd} \tag{B-29}$$

$$i_{sq} = -i_{rq} \tag{B-30}$$

Mechanical equations:

$$T_{em} = -\frac{P}{2}\lambda_{rd}i_{rq} \tag{B-31}$$

$$\omega_{da} = \omega_m + \omega_{dA} = \frac{P}{2}\omega_{mech} + \omega_{dA} \tag{B-32}$$

Power inputs:

$$P_s = v_{sq}i_{sq} = \omega_{da}\lambda_{sd}\,i_{sq} \tag{B-33}$$

$$Q_s = v_{sq}i_{sd} = \omega_{da}\lambda_{sd}\,i_{sd} \tag{B-34}$$

$$P_r = v_{rq}i_{rq} = s\omega_{da}\lambda_{rd}\,i_{rq} \tag{B-35}$$

$$Q_r = v_{rq}i_{rd} = s\omega_{da}\lambda_{rd}\,i_{rd} \tag{B-36}$$

Relationships of stator and rotor powers:

$$\frac{P_s}{P_r} = -\frac{1}{s} \tag{B-37}$$

$$Q_s = \omega_{da}L_m i_{md}^2 - \frac{Q_r}{s} \tag{B-38}$$

APPENDIX C: IM SIMULATION SCRIPT

```
Public Module IM

        ! Steady State Operating Condition
        Public f as Native Double = 60 ! Electrical frequency (Hx)
        Public ωe as Native Double = 2 * π * f ! Electrical frequency (rad/s)
        Public VLLrms as Native Double = 690
        Public s as Native Double = 0.01 ! Rated slip

        ! Induction Motor Parameters
        Public P as Native Double = 6 ! number of poles
        Public  Xm1  as  Native  Double  =  573.33m ! Single-phase magnetizing
reactance
        Public Xm as Native Double = 3 / 2 * Xm1 ! Single-phase magnetizing
reactance
        Public Xls as Native Double = 50m ! Stator leakage reactance
        Public Xlr as Native Double = 47m ! Rotor leakage reactance
        Public Rs as Native Double = 2m ! Stator winding resistance
        Public Rr as Native Double = 1.5m ! Rotor resistance
        Public  Lm1  as  Native  Double  =  Xm1  /  ωe  !  Single-phase  magnetizing
inductance
        Public  Lm  as  Native  Double  =  3  /  2  *  Lm1  !  Per-phase  magnetizing
inductance
        Public Lls as Native Double = Xls / ωe ! Stator leakage inductance
        Public Llr as Native Double = Xlr / ωe ! Rotor leakage inductance
        Public Ls as Native Double = Lm + Lls ! Stator inductance
        Public Lr as Native Double = Lm + Llr ! Rotor inductance
        Public Jeq as Native Double = 70 ! Rotor moment of inertia

        Public ωsync as Native Double = ωe * 2 / P ! Synchonous speed at rated
frequency

        Public ωm as Native Double = (1 - s) * ωe ! Speed at rated slip
        Public Va as Native Double = VLLrms * √2 / √3 ! Phase voltage peak
        Public Vs0 as Native Double = 1.5 * Va

        ! Initial dq Voltages
        Public Vsd0 as Native Double = √2 / √3 * Math:Abs(Vs0)
        Public Vsq0 as Native Double = 0
        Public Vrd0 as Native Double = 0
        Public Vrq0 as Native Double = 0

        Public τr as Native Double = Lr / Rr
        Public A as Double = [[Rs, -ωe * Ls, 0, -ωe * Lm], [ωe * Ls, Rs, ωe *
Lm, 0], [0, -s * ωe * Lm, Rr, -s * ωe * Lr], [s * ωe * Lm, 0, s * ωe * Lr,
Rr]]
        Public Ainv as Double = 1 / A
        ! Initial dq stator and rotor voltages (as row matrix)
        Public Vdq0 as Double = [[Vsd0], [Vsq0], [Vrd0], [Vrq0]]
        Public Idq0 as Double = Ainv * Vdq0 ! Initial dq stator and rotor
currents
```

```
! Retriving individual current from row matrix
Public Isd0 as Native Double = Idq0(1)
Public Isq0 as Native Double = Idq0(2)
Public Ird0 as Native Double = Idq0(3)
Public Irq0 as Native Double = Idq0(4)
! Initial electro magnetic torque
Public Tem0 as Native Double = (P / 2) * Lm * (Isq0 * Ird0 - Isd0 * Irq0)
Public Tl0 as Native Double = Tem0 ! Initial load torque, set equal to
electormagnetic torque for starting from steady state condition
Public Wmech0 as Native Double = (2 / P) * ωm ! Initial rotor mechanical
speed
Public M as Double = [[Ls, 0, Lm, 0], [0, Ls, 0, Lm], [Lm, 0, Lr, 0],
[0, Lm, 0, Lr]]
! dq stator and rotor flux
Public λdq0 as Double = M * [[Isd0], [Isq0], [Ird0], [Irq0]]
Public λsd0 as Native Double = λdq0(1)
Public λsq0 as Native Double = λdq0(2)
Public λrd0 as Native Double = λdq0(3)
Public λrq0 as Native Double = λdq0(4)

Public θs as Native Double ! Initial stator flux angle
Public θVs0 as Native Double ! Initial stator voltage angle

Public σ as Native Double = 1 - Lm * Lm / (Ls * Lr)

! speed loop cross over frequency
Public ωc as Native Double = 10
! current loop cross over frequency
Public ωci as Native Double = 20 * ωc
! loop phase margin
Public φm as Native Double = 60°
Public φmi as Native Double = φm
! outer and inner loop, PI gain values
Public kp as Native Double
Public ki as Native Double
Public kpi as Native Double
Public kii as Native Double
Public k as Native Double

! Parameter initalization function
Public Function Init()
    ! local variables, just for the purpose of computation and are
discarded at end of function call
    Local λsdq0 as Native Double = √(λsd0² + λsq0²)
    Local λrdq0 as Native Double = √(λrd0² + λrq0²)
    Local Isdq0 as Native Double = √(Isq0² + Isd0²)
    Local Irdq0 as Native Double = √(Irq0² + Ird0²)
    Local Vsdq0 as Native Double = √(Vsq0² + Vsd0²)
    Local Vrdq0 as Native Double = √(Vrq0² + Vrd0²)
    Local θλrdq as Native Double = Math:ATan2(λrq0, λrd0) ! rotor
flux space vector angle
```

```
            Local θIsdq as Native Double = Math:ATan2(Isq0, Isd0)
            Local θIrdq as Native Double = Math:ATan2(Irq0, Ird0)
            Local θVsdq as Native Double = Math:ATan2(Vsq0, Vsd0)
            Local θVrdq as Native Double = Math:ATan2(Vrq0, Vrd0)
            Local ωckpbyki as Native Double
            Local ωcikpibykii as Native Double

            θs = Math:ATan2(λsq0, λsd0) ! stator flux space vector angle

            λsd0 = λsdq0
            λsq0 = 0
            λrd0 = λrdq0 * Math:Cos(θλrdq - θs)
            λrq0 = λrdq0 * Math:Sin(θλrdq - θs)
            Isd0 = Isdq0 * Math:Cos(θIsdq - θs)
            Isq0 = Isdq0 * Math:Sin(θIsdq - θs)
            Ird0 = Irdq0 * Math:Cos(θIrdq - θs)
            Irq0 = Irdq0 * Math:Sin(θIrdq - θs)
            Vsd0 = Vsdq0 * Math:Cos(θVsdq - θs)
            Vsq0 = Vsdq0 * Math:Sin(θVsdq - θs)
            Vrd0 = Vrdq0 * Math:Cos(θVrdq - θs)
            Vrq0 = Vrdq0 * Math:Sin(θVrdq - θs)

            Vdq0 = [[Vsd0], [Vsq0], [Vrd0], [Vrq0]]
            Idq0 = [[Isd0], [Isq0], [Ird0], [Irq0]]
            λdq0 = [[λsd0], [λsq0], [λrd0], [λrq0]]

            θVs0 = 90 + Math:ATan2(Vsq0, Vsd0) * 180 / π

            ! outer speed loop PI gain values
            k = -(P / 2) * (Lm / Ls) * λsd0
            ωckpbyki = Math:Tan(φm)
            ki = ωc² * Jeq / (k * √(1 + (Math:Tan(φm))²))
            kp = ki * ωckpbyki / ωc

            ! inner current loop PI gain values
            ωcikpibykii = Math:Tan(φmi - π / 2 + Math:ATan(ωci * Lr * σ /
    Rr))
            kii = ωci * √(Rr² + (ωci * Lr * σ)²) / √(ωcikpibykii² + 1)
            kpi = ωcikpibykii * kii / ωci
        End Function
    End Module
```

APPENDIX D: Sustainable Development Goals (SDGs) ALIGNMENT

This project is related to various of the United Nations Sustainable Development Goals (SDGs):

- #7: Affordable and Clean Energy

Described as "Ensuring access to affordable, reliable, sustainable and modern energy for all", the implementation of DFIGs will surely have a great impact on this goal. As described in this project, the clearest application of these motors are wind turbines, one of the most sustainable and promising clean energy sources that allows humans to generate electricity without contaminating.

- #9: Industry, Innovation and Infrastructure

This goal is defined by the UN as "Building resilient infrastructure, promote inclusive and sustainable industrialization and foster innovation". Sustainable energy sources will surely have a great impact on future infrastructures.

- #11: Sustainable Cities and Communities

Paraphrased as "Making cities and human settlements inclusive, safe, resilient and sustainable". In the same line as before, communities and cities will be healthier if cleaner energy sources substitute the traditional polluting ones. DFIG implementation is one of the many ways that will create these cleaner and desired environments.

- #13: Climate Action

Lastly, the UN states this goal as "Taking urgent action to combat climate change and its impacts". This last objective englobes all that has been explained before, perhaps in the view with the most perspective. Ultimately, many of the SDGs are declared so that on one hand, social injustices are eliminated; and on the other hand, a better planet is left for future generations. Developments in different engineering sectors will clearly have a big part in this last role.